U.S. DEPARTMENT OF ENERGY

Office of ENERGY EFFICIENCY & RENEWABLE ENERGY

Long-Term Performance of Narrow-Band Red Emitters Used in SSL Devices

U.S. Department of Energy—Lighting R&D Program

September 2021

(This page intentionally left blank)

RTI Project Number
0215939.001.001

Long-Term Performance of Narrow-Band Red Emitters Used in SSL Devices

September 2021

Prepared for

U.S. Department of Energy

Through contract with
KeyLogic Systems, Inc.
3168 Collins Ferry Road
Morgantown, WV 26505

Prepared by

Kelley Rountree, Lynn Davis, Michelle McCombs,
Roger Pope, Karmann Mills, and Meghan Hegarty-Craver
RTI International
3040 E. Cornwallis Road
Research Triangle Park, NC 27709

Acknowledgments

This material is based upon work supported by the U.S. Department of Energy's Office of Energy Efficiency and Renewable Energy (EERE) under the National Energy Technology Laboratory (NETL) Mission Execution and Strategic Analysis (MESA) contract, award number DE-FE0025912.

Disclaimer

Nomenclature or List of Acronyms

75OL	operational life test conducted at 75°C
7575	life test conducted at 75°C and 75% relative humidity
°C	degree Celsius
α	decay rate constant in ANSI/IES TM-28-20 model
$\Delta u'$	change in the u' coordinate of chromaticity
$\Delta u'v'$	chromaticity shift or the total change in chromaticity coordinates
$\Delta v'$	change in the v' coordinate of chromaticity
λ	wavelength
λ_{max}	maximum emission wavelength in SPD
λ_o	maximum emission wavelength in deconvoluted spectrum
η	quantum efficiency
µm	micrometers
Φ_e	total radiant flux
$\Phi_{e,\lambda}$	spectral radiant flux at wavelength λ
Φ_v	total luminous flux
A	radiant flux of emitter
ac	alternating current
ANSI	American National Standards Institute
AST	accelerated stress test
B	initialization constant
CCT	correlated color temperature
Cd	Cadmium
CdS	Cadmium sulfide
CdSe	Cadmium selenide
Ce:YAG	Cerium-doped yttrium aluminum garnet
CIE	International Commission on Illumination (*Commission Internationale de l'Éclairage*)
CRI	color rendering index

CSM	chromaticity shift mode
dc	direct current
DOE	U.S. Department of Energy
DUT	device under test
EERE	Office of Energy Efficiency and Renewable Energy
EMC	epoxy molding compound
EQE	external quantum efficiency
FR-4	flame retardant epoxy formulation
ft	foot
FWHM	full-width at half-maximum
GaN	gallium nitride
hr, hrs	hour, hours
IES	Illuminating Engineering Society
I_f	forward current
in	inch
IQE	internal quantum efficiency
K	Kelvin
K_m	maximum spectral luminous efficacy constant
L_{70}	time required for the luminous flux to decay to 70% of the initial value
LED	light-emitting diode
LER	luminous efficacy of radiant flux
LFL	linear fluorescent lamp
LFM	luminous flux maintenance
lm	lumen
lm/W	lumens per watt
mA	milliampere or milliamp
MESA	Mission Execution and Strategic Analysis
MP-LED	mid-power LED
NB	narrow-band

NETL	National Energy Technology Laboratory
NIST	National Institute of Standards and Technology
nm	nanometer
PCB	printed circuit board
pc-LED	phosphor-converted LED
PFS	potassium fluorosilicate
ppm	parts per million
QD	quantum dot
R_f	fidelity index in ANSI/IES TM-30-18
R_g	gamut index in ANSI/IES TM-30-18
RoHS	Restriction of Hazardous Substances Directive 2002/95/EC
RTOL	room temperature operational life
s	asymmetry parameter
SCE	secondary converter emission
SPD	spectral power distribution
SSL	solid-state lighting
t	time
T_j	junction temperature
UL	Underwriter's Laboratory
u′	chromaticity coordinate in the CIE 1976 color space
V	volt
V_λ	spectral luminous efficiency function
v′	chromaticity coordinate in the CIE 1976 color space
V_f	forward voltage
w	emission distribution at half-maximum radiant flux
W	watt
W/nm	watts per nanometer

Executive Summary

Solid-state lighting (SSL) technologies that use light-emitting diodes (LEDs) as illumination sources are efficient at converting electric current into optical radiation with wavelengths (λ) between 380 nanometers (nm) and 740 nm. SSL technologies usually produce a minimal amount of infrared radiation, in contrast to standard illumination technologies such as incandescent lamps that typically emit significant amounts of infrared. SSL technologies do produce waste energy due to inefficiencies in the conversion of electric current to emitted photons. In general, this waste energy manifests as increased LED junction temperatures (T_j) and is often removed from the LED package by a combination of thermal conduction (e.g., heat sink) and convection.

SSL technologies that use traditional phosphor-converted LEDs (pc-LEDs) provide an increase in spectral efficiency over incandescent lamps because almost all of the radiation they produce is in the visible range. However, conventional red phosphors used in white, pc-LEDs have broad emission peaks (full-width at half-maximum [FWHM] near 100 nm) that significantly spill over into the deep red and near-infrared regions (i.e., above 740 nm), where the human eye is not sensitive. By decreasing the FWHM of the red emitter (e.g., using a narrow-band [NB] red emitter) or shifting the red emission peak to lower wavelengths, a significant increase in luminous efficacy and spectral efficiency can be realized with potential impacts to the color rendering properties of the light source. One solution to managing the trade-off between spectral efficiency and color rendering is to use a blue LED pump, a broad emitting green-yellow phosphor, and a NB red emitter. This report focuses on a sampling of available SSL products that use NB red emitters to provide a benchmark of these technologies, and the performances of these NB products are compared in terms of luminous efficacy of radiant flux (LER), color rendering, and correlated color temperature (CCT). Conventional SSL products that use pc-LEDs of similar CCT values are also included in the comparison to investigate the potential energy savings of using NB red emitters instead of phosphors with broader red emission peaks, as is often done in conventional SSL devices.

The selected NB red emitter products investigated in this report used different architectures to decrease deep red and near-infrared emissions. One product was a 2-ft, Type A replacement, LED tube (Product NB-1) that contained magnesium-doped potassium fluorosilicate (PFS) phosphor, a NB technology that was first used in displays. Product NB-1 contains an LED module with 42 mid-power LEDs (MP-LEDs) encased in a glass tube and the product was tested in this form. The other two products (NB-2 and NB-3) that were benchmarked in this study contained red quantum dots (QDs) mixed with conventional green phosphors. QDs have recently made significant market gains in display and television applications. Both Product NB-2 and NB-3 were tested as light engines with two LED modules mounted to a common heat sink. No secondary optics were used with Products NB-2 and NB-3. The LED modules of Product NB-2 contain 21 MP-LEDs whereas the LED modules of Product NB-3 contain 72 MP-LEDs each.

This report summarizes the overall findings from up to 12,000 hours (hrs) of accelerated stress testing (AST) on the Product NB-1 DUTs and up to 11,000 hrs of AST on the Product NB-2 DUTs. The AST procedures used in this study included a room temperature operational life (RTOL) test, an operational life test conducted at 75°C (75OL), and a wet high-temperature operational life test performed at 75°C and 75% relative humidity (7575). Data for Product NB-3 is presented through 7,000 hours of operation in RTOL. During the ASTs described herein, separate populations of each product (three DUTs in each population for Product NB-1 and four DUTs in each population for Product NB-2) were subjected to power cycling of 1 hr on and 1 hr off. Four DUTs for Product NB-3 were operated continuously in RTOL. The performance of these NB products is compared to findings from two downlights that produce spectra that can be switched between different, preselected CCT values (e.g., nominal switching CCT values were 2,700 K, 3,000 K, 3,500 K, 4,000 K, and 5,000 K).

In addition, the light sources from representative samples of all DUTs were decapped using a chemical solution, which allowed an estimation of the external quantum efficiency (EQE) of the blue LED ($\eta_{blue,EQE}$) and the phosphor ($\eta_{phos,EQE}$). The $\eta_{blue,EQE}$ estimate provides a guide to the efficiency of the product in

converting electrical current into emitted photons. The $\eta_{phos,EQE}$ values provide an estimate of the efficiency of blue photon conversion to broadband white light (e.g., green, red).

The key findings from this study include the following:

- The radiant efficiency of the devices incorporating NB phosphors was generally higher than the conventional pc-LED technology benchmarks at all CCT values tested. Further improvements in radiant efficiency of these NB products appear possible with the use of more efficient LED emitters.

- The narrowing of the red emission bands for the products in this study also led to significant gains in LER compared to the conventional pc-LED products. The best LER performance (329 lumens/watt [lm/W]) was found for the PFS samples (Product NB-1) with a nominal CCT of 3,500 K. This LER value represents a 15% improvement over the conventional pc-LED benchmark operated at 3,500 K.

- The QD-containing products (NB-2 and NB-3) also exhibited an increase in LER over the conventional pc-LED benchmarks. The LER performance for the 4,000 K product (Product NB-3) was 310 lm/W (8% improvement over the pc-LED benchmarks at 4,000 K). For the 2,700 K product (Product NB-2), the LER was 294 lm/W, a 2% improvement over the pc-LED benchmarks.

- The EQE value of the phosphor ($\eta_{phos,EQE}$) was estimated to be the highest for the PFS phosphor (0.99). The QD-phosphor composite was estimated to have excellent EQE values for both the 2,700 K and 4,000 K products, although the $\eta_{phos,EQE}$ value was estimated to be higher for Product NB-3 (0.97) than Product NB-2 (0.89).

- The color rendering properties of Products NB-1, NB-2, and NB-3 were excellent ($R_f \geq 91$, $R_g = 99$), supporting the finding that increases in spectral efficiency in the red region can be achieved in a manner that does not adversely impact color rendering.

- The temperature stability of the products in this study was generally good. The luminous flux maintenances (LFMs) of Product NB-1 remained above 0.93 in RTOL and 75OL over the test duration (12,000 hrs). For Product NB-2, the LFM value of the DUTs in RTOL and 75OL remained above 0.97 after 11,000 hrs of testing. Product NB-3 was only tested in RTOL, and its LFM value exceeded 0.99 after 7,000 hrs of testing.

- The magnitude of chromaticity shift ($\Delta u'v'$) remained small for Products NB-1, NB-2, and NB-3 in the RTOL and 75OL test conditions ($\Delta u'v' < 0.001$), demonstrating excellent color stability in these conditions.

- The products in this study were greatly affected by the presence of humidity in the 7575 environment. LFM decreased drastically for both Products NB-1 and NB-2 and reached 0.80 by 6,000 hrs of exposure for Product NB-1 and 0.83 after 9,000 hrs of exposure for Product NB-2. Chromaticity shift also increased substantially for both products, with Product NB-1 (PFS phosphor) experiencing a shift in the blue direction ($\Delta u'v' = 0.005$) after 6,000 hrs and all DUTs of Product NB-2 (phosphor-QD mixture) failing parametrically due to excessive chromaticity shift ($\Delta u'v' > 0.007$) in the green direction by 3,000 hrs.

- The phosphor-QD mixture used in Product NB-2 was especially susceptible to the humid environment of 7575, and the emission peak of the mixture shifted by 10 nm toward a lower value by the end of the test in the 7575 conditions.

The results in this report serve to benchmark the reliability of narrow-band red emitters and direct future research. In this report, narrow-band red emitters are shown to provide significant gains in spectral efficiency without compromising color fidelity. The products studied had good stability in low-humidity environments but improvements can be made in high-humidity environments, particularly for the phosphor-QD mixture.

Table of Contents

List of Figures

List of Tables

1 Introduction

White light-emitting diodes (LEDs) made one of their first appearances in commercial applications as the small backlit displays used in mobile phones and pagers in the 1990s [1]. Today, low-power LEDs are widely used in displays for mobile devices, televisions, and computers with the worldwide market for LED use in display backlighting expected to be approximately $9 billion in 2021 [2]. Historically, many LED technologies have migrated from display applications to general lighting applications. The adoption rates of technologies from display applications to general lighting applications vary and depend in part on whether the technology can meet the higher performance requirements of general lighting. Examples of performance requirements of general lighting include lifetime length, thermal stability, and performance under high photon flux densities.

Two recent narrow-band (NB) red emitter technologies that have transitioned from widespread use in displays into the general lighting market are manganese-doped potassium fluorosilicate (PFS) phosphors and quantum dots (QDs). NB red technologies are sought for display applications to improve color gamut, while NB red technologies are sought for lighting applications predominantly to improve the luminous efficacy of radiant flux (LER) of a device. LER is defined as the quotient of the total luminous flux divided by the total radiant flux and is expressed in lumens per watt (lm/W) [3]. LER is calculated with Equation 1.

$$LER = \frac{\Phi_v}{\Phi_e} = \frac{K_m \int_{380}^{740} \Phi_{e,\lambda} V_\lambda d\lambda}{\int_{380}^{740} \Phi_{e,\lambda} d\lambda} \quad \text{(Eq. 1)}$$

where Φ_e is total radiant flux, Φ_v is total luminous flux, K_m is the maximum spectral luminous efficacy constant for photopic vision, $\Phi_{e,\lambda}$ is the spectral radiant flux at wavelength λ, and V_λ is the spectral luminous efficiency function. Therefore, LER provides a measure of the efficiency of electrical power conversion to visible light, and a higher value of LER denotes increased optical radiation efficiency achieved by using a source that is more closely matched with the photopic sensitivity curve with minimal amounts of non-visible radiation. Consequently, the highest LER values are produced by radiation in the 480 nm to 620 nm spectral range. Radiation above 740 nm does not contribute to photopic vision (i.e., is generally invisible to the human eye and does not contribute to LER) but is manifested as waste heat. Therefore, increasing LER also likely reduces waste heat production from an LED as shown in **Figure 1-1.**

LER is not the only metric that should be considered when choosing a light source. Other metrics such as color gamut (R_g) and color fidelity (R_f), as described in the American National Standards Institute (ANSI)/Illumination Engineering Society (IES) standard ANSI/IES TM-30-20 [4], are also important. While NB emitters are typically desired to improve LER, broader emission peaks usually improve values of R_g and R_f for a light source. Simultaneous optimization of LER, R_g, and R_f can be daunting and usually requires optimization of narrow emissions at specific wavelengths. Therefore, NB red technologies are especially important in optimizing LER, R_g, and R_f because NB emitters can emit light at wavelengths with appreciable LER values and also contribute to increasing R_g and R_f values for a light source.

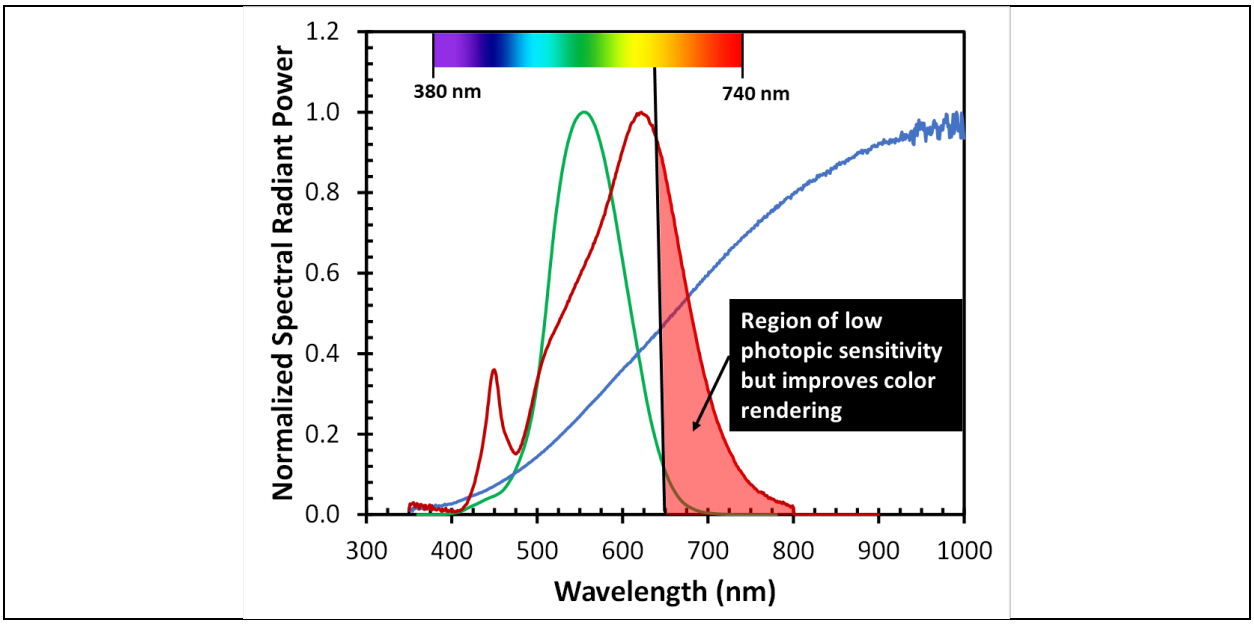

Figure 1-1: Comparison of the spectral emissions from an incandescent lamp (blue), a typical LED lamp (red), and the photopic sensitivity curve (green). All spectra are normalized to a value of 1.0 for the maximum emission wavelength.

1.1 Manganese-Doped Potassium Fluorosilicate Phosphor

Manganese-doped PFS phosphor, also known as KFS phosphor, was one of the first NB red technologies used in the display industry. Through 2018, the technology has been used in over 30 billion LED backlights in commercial display devices [5]. PFS is one of several NB red, manganese-doped, fluoride phosphors of the general composition $A_2[MF_6]:Mn^{4+}$ where A is typically selected from lithium, sodium, potassium, rubidium, cesium, or ammonium and M is typically selected from germanium, silicon, tin, or zirconium [6]. Several fluoride phosphors of this class have been synthesized, and while the location of the emission peaks vary, the emissions generally occur at red spectral wavelengths (i.e., 620–740 nm) [6]. PFS, which has a chemical composition of $K_2SiF_6:Mn^{4+}$, is one of the more prominent fluoride phosphors in this class and has emissions occurring in five narrow bands (full-width at half-maximum [FWHM] is less than 2 nm) between 609 and 648 nm [5].

PFS phosphor has been used as an on-chip solution for low-power and mid-power LEDs (MP-LEDs). The technology is compliant with the Restriction of Hazardous Substances (RoHS) directive established by the European Union [7]. In addition, PFS has a high quantum efficiency (η), with the internal quantum efficiency (IQE) of 3 micrometer (μm)–sized PFS phosphors being about 0.90 [5].

1.2 Quantum Dots

QDs consist of a core containing a nanocrystalline material surrounded by one or more shells of inert material. The most common QDs contain cadmium selenide (CdSe) cores surrounded by cadmium sulfide (CdS) shells [8]. The color of light emitted by the QD depends on the size and chemistry of the core. For CdSe QDs, core sizes range from 2 nm to 5 nm, which produce colors ranging from blue to red, respectively [9]. The size of the QD core can be controlled precisely and is determined by the reaction time used to form the nanocrystal core.

Initial studies of the use of QDs in lighting applications focused on remote-phosphor geometries [10]. Recent advances in QD chemistry have significantly increased the Stokes shift and improved temperature stability, allowing QDs to be used directly on the surface of low-power and MP-LEDs in a proximate phosphor configuration [11]. When measured at room temperature, QDs embedded in silicone can have a η value of up

to 0.90 depending on the QD loading, photon flux levels, and other conditions [12]. When packaged in silicone and placed in a LED package (e.g., 2226 package), the measured luminous efficacy of the LED ranged from 165 lm/W, at a cadmium (Cd) concentration of 90 parts per million (ppm), to 203 lm/W, at a Cd concentration of 600 ppm [13]. The correlated color temperature (CCT) value of these devices was approximately 3,000 K and the color rendering index (CRI) was at least 90. In contrast, a conventional phosphor-converted LED (pc-LED) in the same package had a luminous efficacy of 158 lm/W at a CCT of 3,000 K and CRI of at least 90.

High efficiency QDs are available in a variety of core-shell structures including spherical [14] and asymmetrical [15] QDs. Symmetrical spherical particles with thick CdS shells achieve η values of up to 0.88 at amber and red emission wavelengths. These same materials when encapsulated in silicones and deposited on the surface of blue LEDs produced η values of up to 0.85 and exhibited good performance during life testing of several hundred hours of continuous operation [14]. Optimizing growth conditions to produce asymmetric (e.g., ellipsoidal) core/shell QD structures with the nanocrystalline core located anisotropically in the shell increased the η value to greater than 0.90 due to reduction of trap states in the nanocrystalline core and surround shell [15].

One of the limitations of Cd-based QDs is that Cd is a restricted substance under the RoHS directive, and Cd concentrations are currently limited to less than 100 ppm in electronic materials. The environmental impact of < 100 ppm Cd in LEDs is likely to be small compared to other sources of Cd; however, the regulation is in force. While materials such as indium phosphide are being studied as potential replacements for CdSe QDs, their performance does not currently equal that available with CdSe [12].

1.3 Goals of This Report

This report is the second in a series that examines the long-term performance of commercial LED products containing secondary converters made with either manganese-doped PFS phosphors or QDs. A previous study [16] provided initial benchmarks of the products tested here, and the current study contains accelerated stress testing of these products for up to 12,000 hours of operation.

2 Experimental and Analytical Methods

This report builds on the previous study that provided initial benchmarks of commercial products with NB secondary emitters and compares their performance to traditional pc-LED downlights [16]. The NB products are identified with the nomenclature NB-1, NB-2, and NB-3, while the downlights are denoted as MS-4 and MS-5 where MS stands for mixed spectral output. Products MS-4 and MS-5 are conventional LED phosphor products, and full details can be found elsewhere [17, 18]. Many of the same accelerated stress testing (AST) protocols and measurement methods used during the study and discussed in this report were described previously. In this current report, we provide updated recent experimental findings and long-term trends of the devices under test (DUTs) with secondary converters containing either PFS phosphors or QDs. We are also providing initial results on Product NB-3. A comparison to Products MS-4 and MS-5 is provided to benchmark against standard LED technologies.

2.1 Samples

All products were characterized at both the product level and the LED level. For Products NB-1, MS-4, and MS-5, this involved testing the product with the internal driver supplied by the manufacturer or in a set fixture. For Products NB-2 and NB-3, this involved testing at the LED module level with an external driver. A summary of electrical and optical performance as measured at the LED module level (e.g., nominal CCT, module power, luminous efficacy) and at the individual LED level (e.g., forward voltage [V_f], forward current [I_f]) is given in **Table 2-1**. Pictures of the devices are given in **Appendix A** and the TM-30-15 analysis of the NB products tested in report is given in **Appendix B**. Additional details on each sample are provided in this section of the report.

Products MS-4 and MS-5 DUTs were previously evaluated by RTI and are presented as a comparison spectrum to the narrow-band products [17,18]. These products use a standard warm-white LED with a blue LED pump and an all-phosphor secondary emitter to produce high R_f and R_g values. Products MS-4 and MS-5 also have a switchable CCT value of 2,700 K, 3,000 K, 3,500 K, 4,000 K, and 5,000 K, allowing one lamp to represent many standard solid-state lighting (SSL) products.

Table 2-1: Optical Properties of the SSL Products Examined During This Study.

Label	Narrow-band Emitter	Nominal CCT (K)	Product Power (W_{dc})	Product Luminous Efficacy (lm/W)	V_f of LEDs (V)	I_f of LEDs (mA)
Product NB-1	PFS/KSF	3,500	8.98	150	2.970	96
Product NB-2	QD	2,700	10.1	119	3.26	147
Product NB-3	QD	4,000	23.8	164	2.82	118
Product MS-4	Standard LED Phosphor	2,700 to 5,000[a]	7.47[b]	111[c]	8.467	72
Product MS-5	Standard LED Phosphor	2,700 to 5,000[a]	10.5[b]	107[c]	5.779	169

[a] Products MS-4 and MS-5 have switchable CCT values that can be set to one of five predetermined positions.

[b] Direct current (dc) electrical power that is consumed will depend slightly on switch setting.

[c] Luminous efficacy is quoted only for the 5,000 K nominal setting.

2.1.1 Product NB-1 Additional Details

Product NB-1 is an Underwriter's Laboratory (UL) Type A 2-ft replacement LED tube for traditional linear fluorescent lighting (LFL) as shown in **Figure B-1**. Product NB-1 contains an LED module with 42 MP-LEDs mounted on a rectangular metal-core printed circuit board (PCB). There are two different types of pc-LED packages on the PCB: a yellow-colored phosphor that contains the PFS narrow-band red phosphor and an orange-colored phosphor as shown in **Figure A-2**. The pc-LED with the PFS phosphor has sharp emission peaks at 614 nm, 631 nm, and 636 nm, weaker peaks at 609 nm and 648 nm, and is combined with phosphors that emit broadly in the green and yellow wavelengths (500 nm to 600 nm). The LED packages with an orange-colored phosphor contain a broad emission peak at approximately 595 nm (FWHM is approximately 110 nm) and a smaller green/yellow phosphor emission peak. The entire LED module is encased in a glass tube that mixes the light from the LEDs and provides a 270° light distribution. The different types of pc-LEDs are arranged in an alternating fashion on the PCB, with the first 21 serially connected MP-LEDs connected in parallel to a set of capacitors and the rest of the MP-LEDs (i.e., the second set of 21 serially connected MP-LEDs). The LED tubes are operated with traditional LFL ballasts (plug-and-play), offering quick and low-cost installation.

A compatible LFL ballast suggested by the manufacturer of Product NB-1 was purchased to operate this product. Each LED package is operated at an average of 2.97 V and 96 mA as summarized in **Table 2-1.**

Product NB-1 is rated by the lamp manufacturer for use in damp locations; however, the manufacturer does not provide any information about the maximum use temperature. During our testing, the product housing reached a maximum temperature of 80°C during 7575 (i.e., life test performed at 75°C and 75% relative humidity) exposure.

2.1.2 Product NB-2 Additional Details

Product NB-2 is an LED light engine consisting of two LED modules that were analyzed separately and without any secondary optics. Each LED module was a 1 ft long metal-core PCB that contained 21 MP-LEDs (3030 package size) arranged as three parallel strings of LEDs with seven serially connected LEDs and a

resistor in each string. Product NB-2 MP-LEDs use a blue LED pump, phosphor emissions in the green/yellow spectral region, and a hybrid red phosphor with narrow-band red QDs (a separate peak for the QD emission is not observed due to the limitations of QD concentration by RoHS and λ_{max} of the phosphor-QD mixture is approximately 622 nm). The total voltage across an LED module was 22.9 V, and the total current was 441 mA. Given the arrangement of the LED packages (i.e., three parallel strings of seven serially connected LED packages), this equates to V_f of 3.26 V and I_f of 147 mA across each LED package. Two LEDs were arranged in parallel in each LED package, so the I_f of each LED was 73.5 mA (V_f = 3.26 V). The molding resin for each MP-LED was epoxy molding compound (EMC) per the product's data sheet. For convenience, two LED modules are mounted on the same heat sink as shown in **Figure A-3**. However, there are no secondary optics used with Product NB-2, and each LED module could be operated independently if desired.

Product NB-2 uses a blue LED pump, phosphor emissions in the green/yellow spectral region, and a hybrid red phosphor with narrow-band red QDs (λ_{max} of the phosphor-QD mixture is approximately 622 nm). The manufacturer's specification for the LED packages used in this product are I_f is 180 mA or less, a maximum junction temperature (T_j) of 125°C, and a maximum operating ambient temperature of 100°C. During testing in 7575, the temperature of the LED light engine peaked at 83°C and I_f equaled 147 mA, well within the manufacture's specifications.

Because Product NB-2 was operated by a remote driver that was only used during testing, driver efficiency numbers will change with product configuration. Therefore, they are not reported here.

2.1.3 Product NB-3 Additional Details

Product NB-3 is an LED light engine consisting of two LED modules of 2 ft in length. Each LED module was analyzed separately and without any secondary optics. Each LED module was built on an FR-4 PCB and contained 72 MP-LEDs (3030 package size) arranged as six parallel strings of LEDs with 12 serially connected LEDs. The MP-LEDs utilize EMC as the base polymer for the LED package. For convenience, two LED modules are mounted on the same heat sink as shown in **Figure A-4.** During AST, each LED module on a heat sink was connected to an LED driver that was placed outside the test chamber. In this configuration, the driver delivered 23.8 W (33.8 V at 706 mA) to the LEDs, indicating that the V_f supplied to each individual LED package is 2.82 V and the I_f is 118 mA as summarized in **Table 2-1**. There are two LEDs in parallel in each LED package, indicating that the V_f supplied to each LED is 2.82 V and the I_f across each LED is 59 mA.

Product NB-3 uses a blue LED pump, phosphor emissions in the green/yellow spectral region, and a hybrid red phosphor with narrow-band red QDs (λ_{max} of the phosphor-QD mixture is approximately 618 nm) as shown in **Figure B-2**. Because the total amount of QDs introduced into the phosphor-QD mix is limited by RoHS, a separate emission peak from the QDs is not found in the spectrum. The emissions from the QDs blend into the phosphor emission peak to create a continuous spectrum with reduced emissions at red wavelengths where photopic sensitivity is lower (e.g., 650–740 nm). The light produced by the product exhibited excellent R_f and R_g values (91 and 99, respectively as shown in **Figure B-2**).

The manufacturer's specification for the LED modules used in this product are I_f of 1,080 mA or less, a maximum solder-point temperature (T_{sp}) of 105°C, and a maximum operating ambient temperature of 130°C. Because Product NB-3 was operated by a remote driver that was only used during testing, driver efficiency numbers will change with product configuration. Therefore, they are not reported here.

2.1.4 Product MS-4 Additional Details

Product MS-4 is a 6-inch downlight with an integrated driver contained in an aluminum housing (**Figure A-5**). The device contains two LED primaries, one with a nominal CCT value of 2,700 K and the other with a nominal CCT value of 5,000 K. By changing a switch on the back of the product, the current distribution between the two LED primaries can be altered, and the CCT value of light produced by the lamp adjusted in discrete steps. This analysis will only compare the narrow-band phosphors to the 2,700 K, 3,500 K, and 4,000 K settings of this product, which are similar to the CCT values of Products NB-2, NB-1, and NB-3,

respectively. Further device details about Product MS-4 and its full evaluation can be found in our previous reports [17,18]. The maximum dc power delivered to an LED primary is 7.47 W. There are nine emitters in each LED package (arranged as three parallel strings of three serially connected emitters), and the I_f across each LED package is 72 mA (V_f = 8.467 V, see **Table 2-1**).

2.1.5 Product MS-5 Additional Details

Product MS-5 is a 6-inch downlight with an integrated driver contained in an aluminum housing (**Figure A-6**). The device contains two LED primaries, one with a nominal CCT value of 2,700 K and the other with a nominal CCT value of 5,000 K. By changing a switch on the back of the product, the current distribution between the two LED primaries can be altered and the CCT value of light produced by the lamp adjusted in discrete steps. This analysis will only compare the narrow-band phosphors to the 2,7000 K, 3,500 K, and 4,000 K settings of this product, which are similar to the CCT values of Products NB-2, NB-1, and NB-3, respectively. Further device details about Product MS-5 and its full evaluation can be found in our previous reports [17,18]. The maximum power delivered to the 2,700 K LED primary was approximately 10.5 W, which is distributed as a V_f of 5.78 V (two LEDs in series in the LED package) and an I_f of 169 mA for each LED at full power (see **Table 2-1**).

2.2 Stress Testing Methods

The samples of each product were separated into three populations, and each population was tested in one of three possible conditions: room temperature operational life (RTOL), an operational life test at an elevated ambient temperature of 75°C (75OL), or an operational life test at 75°C and 75% relative humidity (7575). Either a temperature oven or a temperature-humidity environmental chamber was used for these tests, but humidity was not explicitly controlled in RTOL or 75OL (ambient humidity was determined by the air handling system of the building). For the LED tubes (Product NB-1), the population test size for each of the conditions was set to three DUTs. For the light engines (Product NB-2 and NB-3), two light engines containing two LED modules each were tested, giving four DUTs for each testing protocol. Products NB-1 and NB-2 were power cycled for 1 hour (hr) on and 1 hr off and Product NB-3 was operated continuously.

For this study, Product NB-1 was mounted to a traditional 2-ft T8 LFL fixture, and the DUTs were operated with a traditional LFL ballast recommended by the lamp manufacturer. The LFL ballast was stored within the LFL fixture and therefore experienced the AST protocol with the Product NB-1 DUTs. Product NB-2 used a single aluminum heat sink to mount two LED modules. The LED modules were connected in series to a driver that was placed outside the test chamber. Product NB-3 has two LED modules on the same heat sink with separate external drivers for each module.

2.3 Measurement and Analytical Methods

2.3.1 Luminous Flux

The spectral power distribution (SPD), luminous flux, and chromaticity measurements of all samples were taken at room temperature in a calibrated 65-in integrating sphere. Products NB-1, NB-2, and NB-3 were mounted in the center of the sphere (4π geometry), and Products MS-4 and MS-5 were mounted on the exterior of the sphere facing inward (2π geometry). During photometric testing in the 4π geometry, the center post supplied alternating current (ac) power to the 2-ft T8 LFL fixture and accompanying ballast for Product NB-1. The center post also provided dc power (from the external driver) to Products NB-2 and NB-3. A control electrical driver (not exposed to test conditions) was reserved for all photometric tests for Products NB-1, NB-2, and NB-3 so that electrical losses due to the driver were comparable. Product MS-4 was mounted external to the integrating sphere, and the internal driver in each DUT was powered by line ac. Regular calibrations of the integrating sphere were performed using a calibrated spectral flux standard (for 4π configuration) or a forward flux standard (for 2π configuration) that was traceable to standards from the National Institute of Standards and Technology (NIST). Background corrections were applied prior to calibration. Self-absorption corrections were made for all samples using an auxiliary lamp mounted inside the sphere, which is in accordance with procedures in ANSI/IES LM-79-19 [19].

2.3.2 Power Measurements

The electrical characteristics of the DUTs examined in this study were measured when needed with a Xitron 2802 two-channel power analyzer. An unexposed driver of the same product was used as a control and measured concurrently. In obtaining the power characteristics, the driver and LED loads were configured as for the AST experiments except that output power connections supplied by the LFL ballast (Product NB-1) or external driver (Products NB-2 and NB-3) were made to the power analyzer to measure the output ac power (Product NB-1) and output dc power (Products NB-2 and NB-3) supplied by the driver to each product. To measure the dc across the pc-LEDs of Product NB-1, one of the pc-LEDs was removed and replaced with electrical wire to pass into the ammeter of the power analyzer.

2.3.3 Emission Spectra

The NB red-emitting products in this report use blue LED(s), green phosphor, and narrow-band red emitters to create white light. Therefore, the decay rate constant (α) determined from ANSI/IES TM-28-20 that describes the degradation of the NB products over time incorporates the rate of degradation of each emitter and all other components of the LED package and system into a single variable. While this information is helpful to project luminous flux maintenance, it does not give information about the contribution of individual emitters to the overall rate. To estimate the contribution from each emitter to the overall decay rate, the SPD was deconvoluted into individual emitters of blue, green, and red colors. The decay rates determined for each emitter of the deconvoluted spectra still incorporate LED package and system decays. All products in this report use a wide-band red phosphor in conjunction with a NB red-emitting material to produce emissions in the red wavelength regions. In the case of the PFS phosphor product (i.e., Product NB-1), the contribution directly from the NB red emitter can be deduced readily from the SPD and literature [5,6]. For the products that use QDs to achieve narrow-band red emission (i.e., Products NB-2 and NB-3), a spectrum is known for the red phosphor and QD mixture [13].

In this report, we deconvolute the SPDs of the QD-containing products (i.e., Products NB-2 and NB-3). A single, skewed emission distribution (commonly called a skewed Gaussian) provided the best fit for the red phosphor-QD mixture emission. An empirical function [$f(s,A,\Delta\lambda,\lambda_o,\lambda]$ to describe a skewed Gaussian can be drawn from Fraser and Suzuki [20] and is shown in Equation 2.

$$f(s, A, \Delta\lambda, \lambda_0, \lambda) = A * \exp\left(-ln(2)\left(ln\left(1 + \frac{2s(\lambda-\lambda_0)}{\Delta\lambda}\right) * \left(\frac{1}{s}\right)\right)^2\right) \quad \text{(Eq. 2)}$$

In Equation 2, A describes the maximum radiant flux of the emitter, λ_0 describes the wavelength at which maximum emission occurs in the deconvoluted spectrum, and s is the asymmetry parameter. The asymmetry parameter is positive when the emission skews at wavelengths $\lambda > \lambda_0$ and negative when the emission skews toward wavelengths $\lambda < \lambda_0$ (for s close to zero, the skewed distribution tends toward a symmetric Gaussian). The relationship between $\Delta\lambda$ and the full width of the emission distribution at half-maximum radiant flux (w) is described in Equation 3, as follows:

$$w = \Delta\lambda\left(\frac{\sinh(s)}{s}\right) \quad \text{(Eq. 3)}$$

Using the known normalized spectrum of the red phosphor-QD mixture, the values of Equations 2 and 3 (i.e., s, A, λ_0, and w) were determined by minimizing the sum of squared errors through a non-linear regression analysis.

With most conventional pc-LEDs, the blue emissions from the LED pump can be modeled with a logistic power peak function [21]. However, due to emissions from two sites of slightly different energies, the blue emissions were better modeled with two skewed Gaussian [22]. To complete the spectral deconvolution of Products NB-2 and NB-3, the green phosphor emission was deduced by assuming a single asymmetric Gaussian peak represented all green emissions. The amplitude of radiant flux (A) for the red phosphor-QD

mixture was permitted to float while the green phosphor peak was being assigned because its concentration (and therefore magnitude of emission) was not known. The resulting deconvolution for an initial SPD of a Product NB-2 DUT is presented in **Figure2-1a**. Because Product NB-3 had LED packages from the same family but at a higher CCT value, the same parameters were used to describe the blue and red emitters while the green emitter changed. The resulting deconvolution for an initial SPD of a Product NB-3 DUT is presented in **Figure2-1b**.

For green and red emitters, radiant power was estimated by using the trapezoid rule to approximate the definite integrals of the skewed Gaussian that composed the SPD. For the blue emission, radiant power was calculated as the sum of definite integrals (also calculated using the trapezoid rule) of the two skewed Gaussian functions.

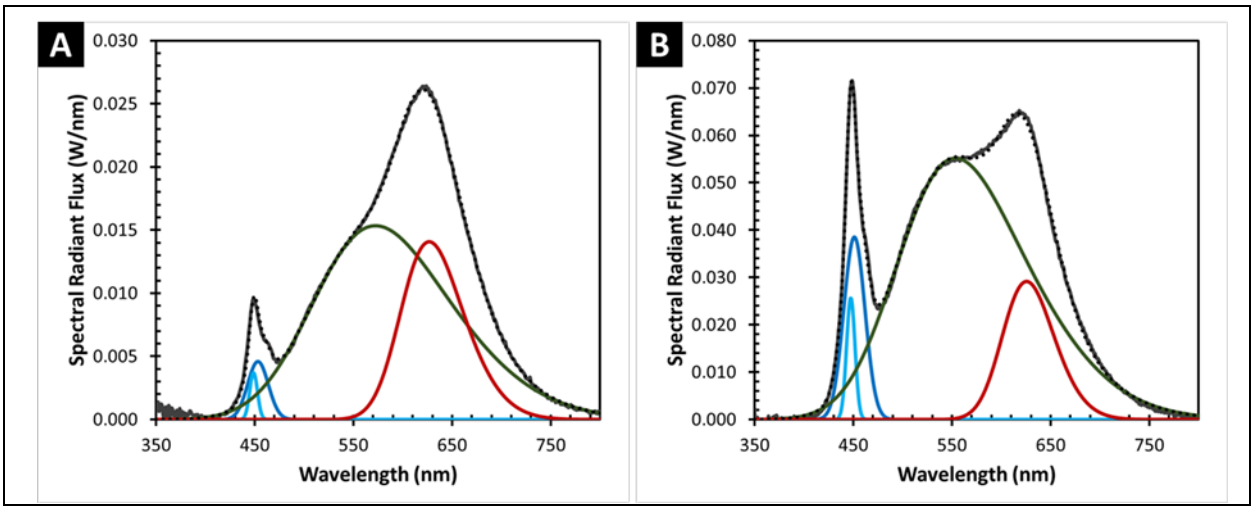

Figure 2-1: Spectral deconvolution of the initial emissions (gray trace) from A) Product NB-2 and B) Product NB-3. The blue, green, and red traces represent the individual emitters while the dotted black line represents the model.

2.3.4 Silicone Decapping Methods

One of the goals of this study was to compare the external quantum efficiency (EQE) of the different narrow-band phosphors with those of conventional nitride phosphors used on most LEDs. To conduct this analysis, the silicone and phosphor layers surrounding the LEDs needed to be removed through decapping. The LED packages were decapped using a standard silicone decapping reagent. Decapping was performed only after removing the LED modules from the product. This required breaking the glass globe for Product NB-1 and removing the LED modules for Products MS-4 and MS-5. Since there were unused LED modules for Product NB-3, one LED module was decapped. For Product NB-2, there were no unused LED modules, but there were individual LEDs from the original tape and reel. Consequently, single LEDs were decapped for Product NB-2.

The decapping operation consisted of a series of solutions. First, the devices were immersed in water for 5 seconds, then dunked in a degreasing solution (eOx Economic Cleaner and Degrease) for 5 seconds. Then the LED module was immersed in the decapping agent (PolyGone 505) and ultrasonicated for 10 minutes. After ultrasonication, the LED module was removed from the decapping agent bath, rinsed with water for 5 seconds, dunked in the degreasing solution for 5 seconds, and rinsed again in water for 5 seconds. Upon completion of the process, each LED module was inspected with an Olympus SZ61 stereomicroscope (zoom range 0.67x to 4.5x) to ensure that the silicone and phosphors had been removed. The microscope is equipped with an Olympus SC30 camera that allowed photography of the decapped LEDs to study the structure inside the package. Select images are shown in **Appendix C** and the SPDs from the decapped DUTs are given in **Appendix D**.

Once the LED modules were decapped, the EQE of a blue LED emitter can be calculated using Equation 4.

$$\eta_{blue,EQE} = \frac{number\ of\ blue\ photons\ emitted}{number\ of\ electrons\ injected\ into\ LED} \quad \text{(Eq. 4)}$$

The number of blue photons emitted from an LED can be calculated from radiometric measurements of the device in an integrating sphere. The total Φ_e value measured in the integrating sphere must be divided by the number of emitters to obtain the average Φ_e value of a single emitter. The number of electrons injected into the LEDs can be determined through electrical measurements and must also be corrected for the number of emitters

In calculating the $\eta_{blue,EQE}$, it is essential to account for the number of LED emitters in the package to obtain the correct number of emitted photons and injected current per LED emitter. These values can be determined by an examination of the optical images of the LEDs (**Appendix C**) and are summarized in **Table 2-2**. Some products had a single LED emitter on each die, and some products incorporated two die in a single package. In these cases, the two LED die are connected in parallel for Products NB-2 and NB-3 and in series for Product MS-5. For Product MS-4, there is only one die in the LED package but multiple LED emitters are integrated into the single die.

Table 2-2: Number of die and emitters per LED package for the studied products.

Sample	LED Package Size	Number of Die per LED Package	Number of LED Emitters per Package	Emitter Connection in Package
NB-1	3 mm x 2.7 mm	1	1	Single emitter
NB-2	3 mm x 3 mm	2	2	Two die connected in parallel
NB-3	3 mm x 3 mm	2	2	Two die connected in parallel
MS-4	3 mm x 2.5 mm	1	9	9 emitters connected as 3 in series and 3 in parallel
MS-5	3 mm x 3 mm	2	2	Two die connected in series

Once $\eta_{blue,EQE}$ is known, the EQE of the phosphor ($\eta_{phos,EQE}$) can be determined using Equation 5.

$$\eta_{phosphor,EQE} = \frac{number\ of\ photons\ emitted\ by\ the\ secondary\ converter}{number\ of\ blue\ photons\ absorbed\ by\ the\ phosphor} \quad \text{(Eq. 5)}$$

The number of photons emitted by the secondary converter can be calculated through integration of the SPD over the phosphor wavelength region (i.e., 495 nm to 800 nm). In this study, the integral of the SPDs was approximated by the trapezoid rule. The number of blue photons absorbed by the phosphor is the number of blue photons emitted by the LED minus the number of unconverted blue photons in the final SPD.

3 Results

In this section, we report the luminous flux maintenance (LFM) and chromaticity maintenance of Products NB-1, NB-2, and NB-3 in various AST protocols. The data presented in this report provide an update for Product NB-1 through 12,000 hrs of operational exposure to RTOL and 75OL. We also show the data for the 7575 test condition for the DUTs of Product NB-1 for completeness, although there are no new data since the last report [16] because all DUTs failed by 8,000 hrs of testing. Updated results for Product NB-2 (through up to 10,000 hrs of operational exposure in RTOL, 75OL, and 7575 tests) and initial findings for Product NB-3 (through up to 6,000 hrs of operational exposure in RTOL conditions) are provided. During the test duration of this report, three abrupt failures occurred (all three Product NB-1 DUTs operated in 7575 failed abruptly due to plastic cracking near the T8 connection); however, many parametric failures occurred due to excessive chromaticity shift including all DUTs operated in the 7575 test conditions for Product NB-2. Since

chromaticity shift failure occurred as early as 2,000 hrs for Product NB-2, we decided to continue testing the DUTs after parametric failure occurred to study long-term LFM and chromaticity shift patterns in these products.

3.1 Product NB-1

3.1.1 Luminous Flux Maintenance

The LFM of Product NB-1 was measured by photometrically testing the DUTs after each 1,000 hrs of operational exposure in the RTOL, 75OL, and 7575 environments according to ANSI/IES LM-84-20 [23]. The results were analyzed using ANSI/IES TM-28-20 [24], and the findings are presented in **Figure 3-1.** Through 8,000 hrs of operation in either RTOL or 75OL, there was a slight increase in LFM (LFM = 1.00 ± 0.01). While the LFM remained very stable and similar for both RTOL and 75OL environments through 8,000 hrs, the 75OL DUTs started experiencing lower LFM relative to the RTOL test population beginning at 9,000 hrs. The decrease in LFM for the 75OL DUTs led to a five-fold increase in the decay rate constant (α) of the 75OL DUTs relative to RTOL. The α values for both RTOL and 75OL DUTs were small, however, and LFM remained high (LFM > 0.95) for both populations through 12,000 hrs. The TM-28-14 projected time to L_{70}(12k) for both RTOL and 75OL test populations is greater than 36,000 hrs, and this projection is limited by the three times rule of ANSI/IES TM-28-20 [24] due to sample size (i.e., the time required to reach L_{70} cannot be projected past three times the actual test interval based on three samples in a test population). The stability of the Product NB-1 DUTs in RTOL and 75OL through 12,000 hrs continues to support that temperature does not have a significant impact on the emitters for ambient temperatures in the 25°C to 75°C range. The increase in luminous flux degradation from 75OL to 7575 suggests that humidity is primarily responsible for the observed accelerated luminous flux degradation. The TM-28-14 projected time to L_{70}(6k) for the 7575 test population was 9,900 hrs.

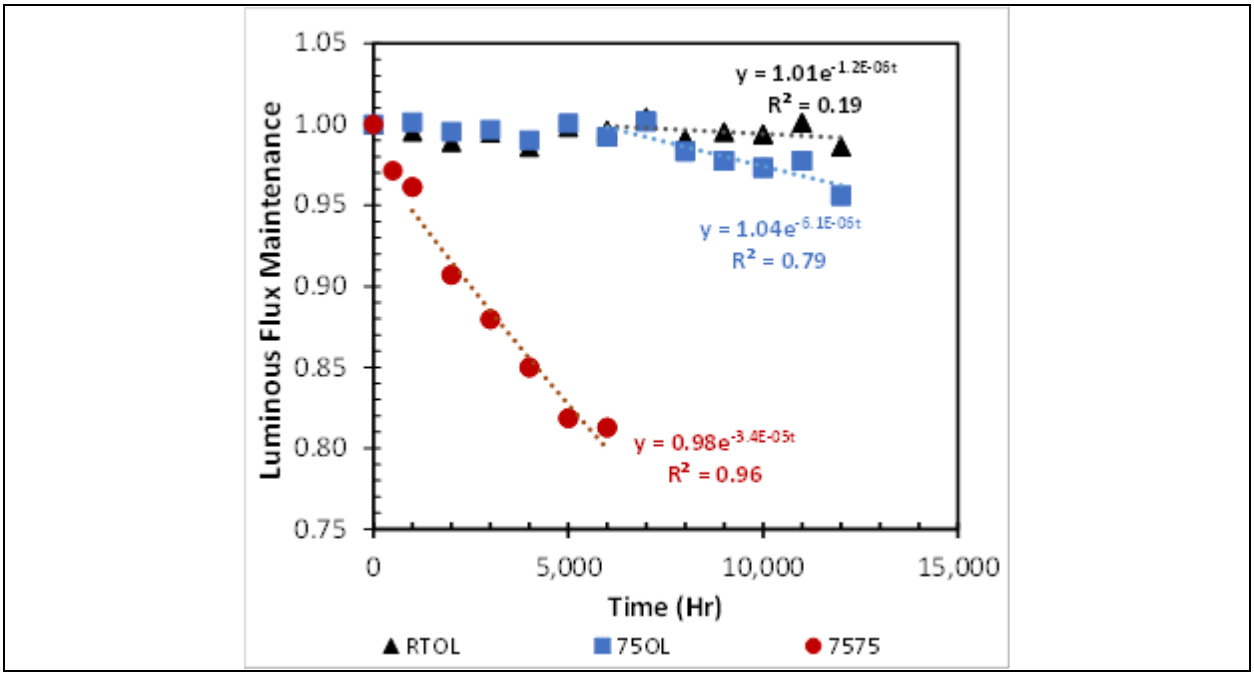

Figure 3-1: LFM of Product NB-1 during RTOL, 75OL, and 7575 according to ANSI/IES LM-84-20 and ANSI/IES TM-28-20.

3.1.2 Chromaticity Maintenance

At ambient and elevated temperatures (i.e., RTOL and 75OL), Product NB-1 had good chromaticity maintenance through 12,000 hrs as shown in **Figure 3-2.** Both test populations experienced a very small,

initial shift in the blue direction (-$\Delta v'$),[1] followed by a slight shift in the green (-$\Delta u'$) or green-yellow (-$\Delta u'$, +$\Delta v'$) directions. The shift in the green direction occurred around 5,000 hrs for the RTOL test population, and the shift in the green-yellow direction occurred at 2,000 hrs for the 75OL test population. The change in chromaticity coordinates of the RTOL and 75OL test populations was slow and constant, and the magnitude of chromaticity shift was small ($\Delta u'v' < 0.0014$). As written in our previous report, humidity had a larger impact than temperature on chromaticity shift behavior for the Product NB-1 DUTs after 6,000 hrs of 7575 exposure ($\Delta u'v' = 0.0053$). The chromaticity shift of the 7575 DUTs was in the generally blue direction (chromaticity shift mode [CSM]-1 mechanism) [25,26]. The blue shift was caused by a decline in the phosphor emissions from green to red wavelengths (500 to 700 nm), leading to a relative rise in blue emissions. The decline in phosphor emissions was accelerated by humidity as indicated by the difference in behavior between 75OL and 7575 suggesting that humidity may affect the long-term quantum efficiency of the phosphors.

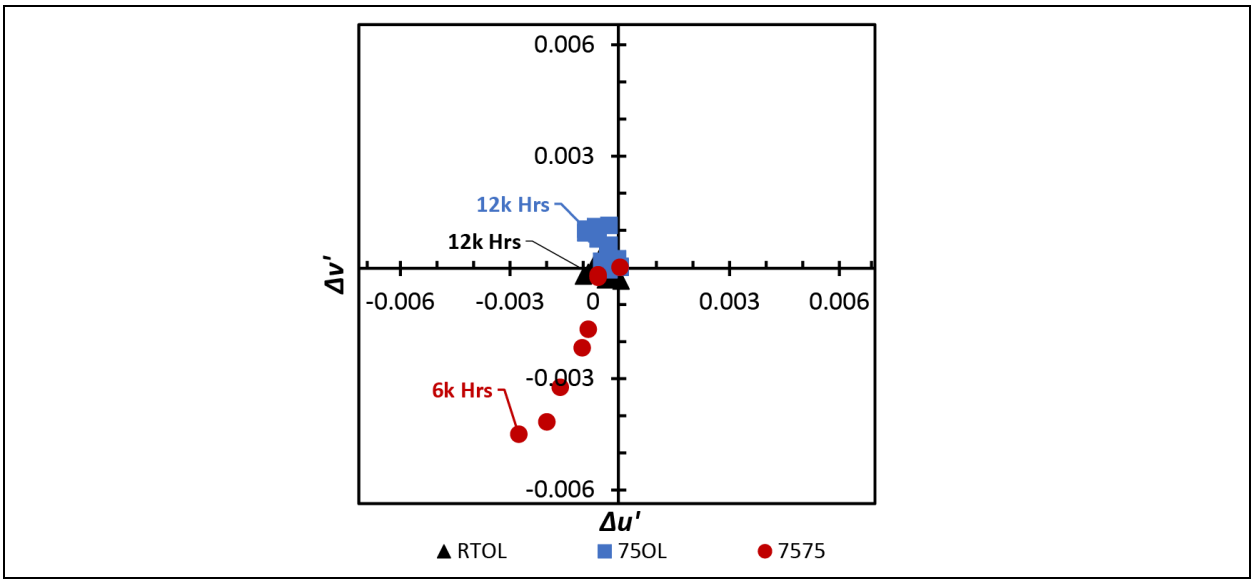

Figure 3-2: Chromaticity shift of Product NB-1 during RTOL, 75OL, and 7575.

3.2 Product NB-2

3.2.1 Luminous Flux Maintenance

Photometric testing was performed on Product NB-2 after each 1,000 hrs of exposure to the RTOL, 75OL, and 7575 environments in accordance with the ANSI/IES LM-84-20 method [23] to determine LFM values. The results were analyzed using an exponential decay model as called for in ANSI/IES TM-28-20 [24], and the findings are presented in **Figure 3-3**. At ambient and elevated temperatures (i.e., RTOL and 75OL), Product NB-2 continued to show minimal luminous flux degradation (LFM > 0.99) over the entire test duration (10,000 hrs). The α values were negligibly different between RTOL and 75OL, which continues to support that the emitters in Product NB-2 do not have much temperature sensitivity at ambient temperatures in the 25°C to 75°C range. The TM-28-14 projected time to L_{70}(10k) for both RTOL and 75OL test populations is greater than 40,000 hrs, which is limited by the four times rule due to sample size.

The Product NB-2 DUTs experienced a large reduction in luminous flux when humidity was introduced to the environment (i.e., 7575). The 7575 DUTs experienced a large, initial drop in luminous flux through 2,000 hrs and then a slower (but significant) decay in luminous flux from 3,000 hrs to 7,000 hrs. The LFM remained

[1] $\Delta u'$ = change in the u' chromaticity coordinate and $\Delta v'$ = change in the v' chromaticity coordinate.

stable from 7,000 hrs to the end of test (LFM = 0.83 at 9,000 hrs). We previously reported that the initial drop in luminous flux was accompanied by a large green shift ($-\Delta u' = 0.007$, $-\Delta v' = 0.001$) that was caused by changes to the phosphor emission peak toward lower intensities and lower wavelengths. The changes to the phosphor peak continued throughout the test at a smaller magnitude than the initial change and will be discussed in more detail in **Section 3.2.2**. The decay rate constant ($\alpha = 2.0 \times 10^{-5}$) increased by seven to ten times for the 7575 DUTs relative to the 75OL and RTOL DUTs, respectively. The TM-28-14 projected time to L70 for the 7575 test population is 17,960 hrs.

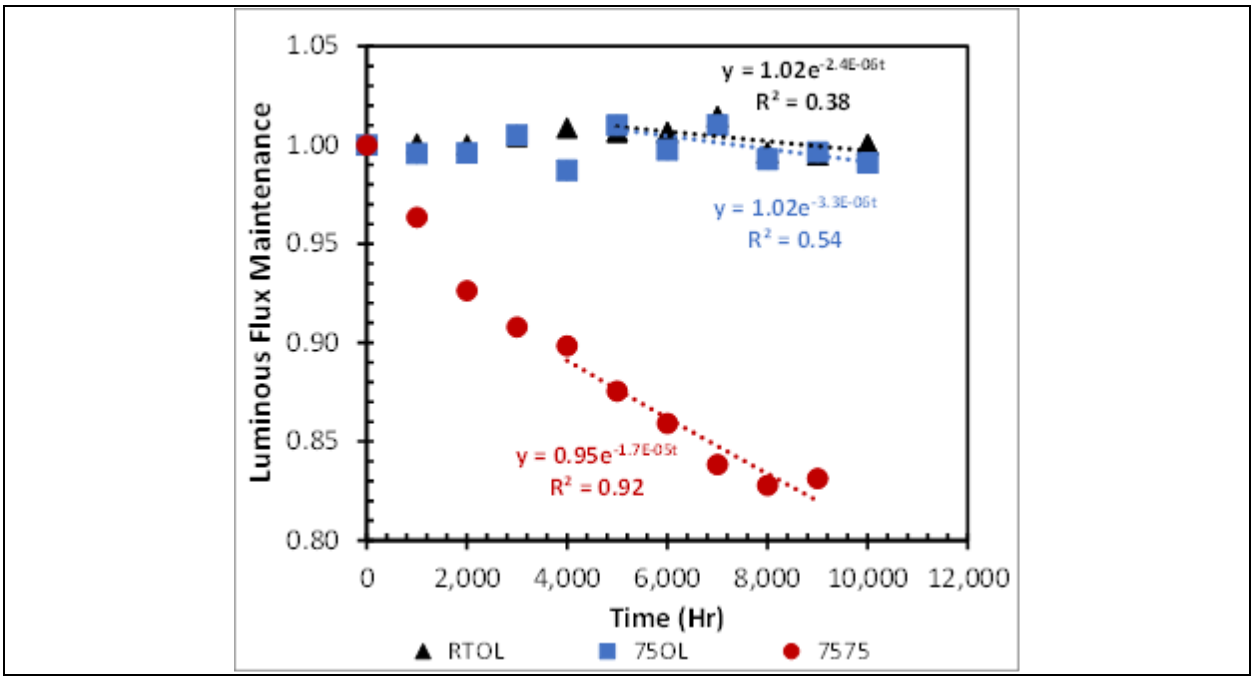

Figure 3-3: LFM of Product NB-2 during RTOL, 75OL, and 7575 according to ANSI/IES LM-84-20 and ANSI/IES TM-28-20.

3.2.2 Chromaticity Maintenance

In both RTOL and 75OL test conditions, the chromaticity coordinates of Product NB-2 DUTs remained stable through 10,000 hrs as shown in **Figure 3-4**. The magnitude of chromaticity shift was minimal for the RTOL and 75OL DUTs ($\Delta u'v' < 0.001$) during the entire test duration. However, when humidity was introduced in the 7575 environment, the Product NB-2 DUTs exhibited large chromaticity shifts. The chromaticity shifted in the green direction mostly along the $-\Delta u'$ axis through 5,000 hrs and then started to shift mostly along the $-\Delta v'$ axis (i.e., in the blue direction). The magnitudes of the chromaticity shifts for the 7575 DUTs was significant: all four DUTs failed parametrically by 3,000 hrs (i.e., $\Delta u'v' > 0.007$) due to excessive chromaticity shift and by 9,000 hrs, the magnitude of chromaticity shift was almost two times greater than the acceptable shift ($\Delta u'v' = 0.013$ at 9,000 hrs).

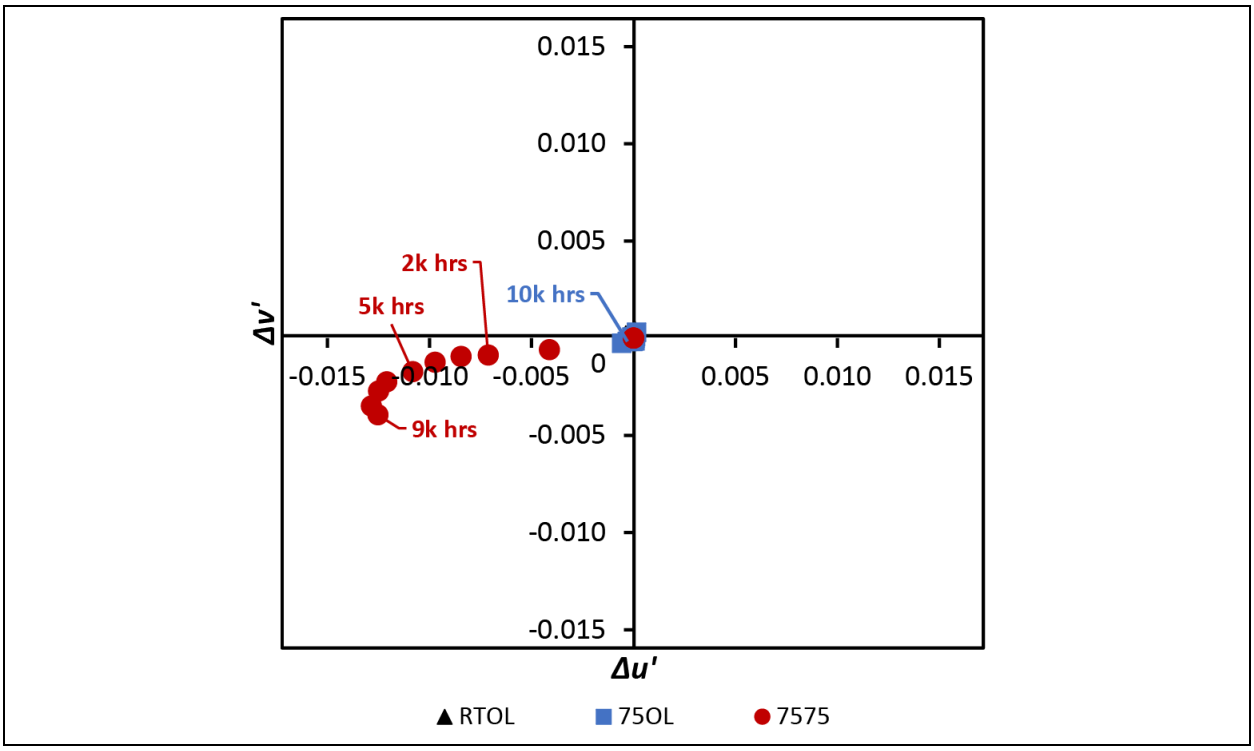

Figure 3-4: Chromaticity shift of Product NB-2 during RTOL, 75OL, and 7575.

The chromaticity shift of the 7575 DUTs in the green direction along the *-Δu'* axis was explained initially in our previous report and an update is provided. In this current report, we found that the secondary converter emission (SCE) continued to be greatly reduced and the secondary emission peak maximum (λ_{max}) still shifted toward lower wavelengths as shown in **Figure 3-5a**. The λ_{max} of the SCE was assigned as the wavelength where maximum radiant flux occurred in the 475–750 nm wavelength region. The SCE includes a green phosphor material and the red emissions from the QD-phosphor emitter. A temporal observation of the SCEs revealed a plateau between 4,000 and 6,000 hrs where the λ_{max} value of the emission peak remained stable, and then the λ_{max} emission peak began moving toward lower wavelengths through 9,000 hrs. There was no change in λ_{max} values for DUTs operated in RTOL and 75OL environments (**Figure 3-5b**). The shift in λ_{max} for the phosphor materials suggests a change in the properties of one or more emitters.

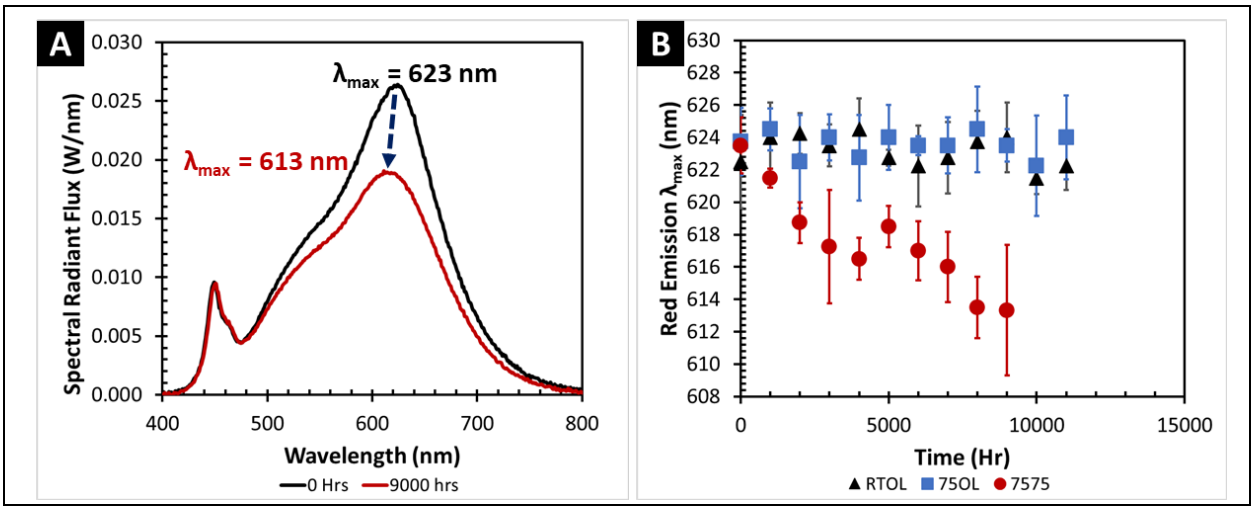

Figure 3-5: Product NB-2 (A) SPD as initially measured and after 9,000 hrs of 7575 exposure and (B) average red emission peak maxima for the DUTs subjected to the different ASTs. The average red emission peak maxima in the 7575 conditions changed throughout testing while no noticeable change occurred in RTOL and 75OL environments, suggesting phosphor and QD oxidation and degradation was largest in the high-humidity environment.

To try to understand whether the change in SCE for Product NB-2 was caused by changes to the green phosphor, red-emitting QD-phosphor mixture, or a combination thereof, the measured SPDs were deconvoluted into blue, green, and red components as outlined in **Section 2.3.3**. It is suspected that either the green phosphor or the QD-phosphor composition was changing with time, so the parameters of the skewed Gaussian (i.e., A, λ_0, s, and w) for the green and red emitters were not fixed during the deconvolution. The initial (t = 0 hrs) and final (t = 9,000 hrs) parameters of the skewed Gaussian for the green and red emitters are provided in **Table 3-1**. The model predicts larger peak wavelength (λ_0) shifts for the green emitter relative to the red phosphor-QD emitter (approximately 11 nm vs. 5 nm, respectively). These λ_0 shifts equate to λ_{max} shifts toward lower wavelengths of approximately 13 nm and 1.0 nm, respectively, when the s and w parameters are incorporated. For the blue emitters, only the amplitudes of the logistic power peak functions were changed (i.e., the peak shape parameters were not changed because the blue emitters were not believed to have any composition changes).

Table 3-1: Parameters of the skewed Gaussian curves used to model the green and red emitters for Product NB-2 in the 7575 test environment.

Parameter	Green Phosphor (0 hrs)	Green Phosphor (9,000 hrs)	QD-phosphor (0 hrs)	QD-phosphor (9,000 hrs)
A	0.015	0.011	0.014	0.010
λ_0	516.5 nm	505.1 ± 1.1 nm	601.9 nm	596.7 ± 0.4 nm
s	2.25	2.56 ± 0.10	2.13	2.17 ± 0.04
w	244.5 nm	240.6 ± 1.0 nm	109.4 nm	128.6 ± 1.1 nm

An examination of the normalized temporal radiant power derived from the deconvoluted spectra is presented in **Figure 3-6**. The radiant power of each emitter was fit with an exponential curve to determine a decay rate, and the average decay rates of each emitter for the 7575 test population are shown in **Table 3-2.** The green phosphor experienced rapid loss of radiant power, dropping to approximately 80% of its initial value, through 4,000 hrs. After the initial period of decay, the radiant power of the green phosphor continued to decay but at a

much slower rate. These two regions of decay for the green emitter suggest two different decay mechanisms or decay pathways in the green phosphor material. The red emitter experienced an initial, small loss in radiant power by 1,000 hrs. From 1,000 hrs to 4,000 hrs, the radiant power of the red emitter remained stable but from 4,000 hrs to the end of test, the radiant power of the red emitters started slowly decaying. The blue LEDs had an initial increase in radiant power to 1,000 hrs at which point the radiant power plateaued. The radiant power of the blue emitters then started increasing again from 4,000 hrs to the end of test (i.e., 9,000 hrs). The increase in emissions from the blue LEDs suggests that a change to the LED package (e.g., a crack in the silicone) may have caused blue LED photons to bypass the phosphor layer.

The chromaticity coordinates (and subsequent chromaticity shift) experienced by the Product NB-2 DUTs in 7575 is dominated by a complex combination of green phosphor oxidation (like that observed in nitride and oxynitride phosphors [27,28], peak wavelength shifts as shown in **Figure 3-5a**) and degradation of the green phosphor material (**Figure 3-6**). In the first 5,000 hrs, the changes that occurred to the green phosphor shifted its peak wavelength to lower values, and even though much radiant power was lost, the overall chromaticity shifted in the green direction. After 4,000 hrs, the radiant power for the blue LEDs started increasing while the radiant power for the green and red emitters experience a more steady-state decay. The combination of these events led to the final chromaticity shift in the blue direction. The λ_{max} values of QD-phosphor mixture did not undergo substantial change in the 7575 test, so we believe that the main cause of lower luminous flux for the red emitter was a combination of degradation (caused by moisture and oxygen ingress [10,11,13,14,29]) and less blue light pump photons (due to LED package changes causing the blue LED photons to bypass the phosphor layer).

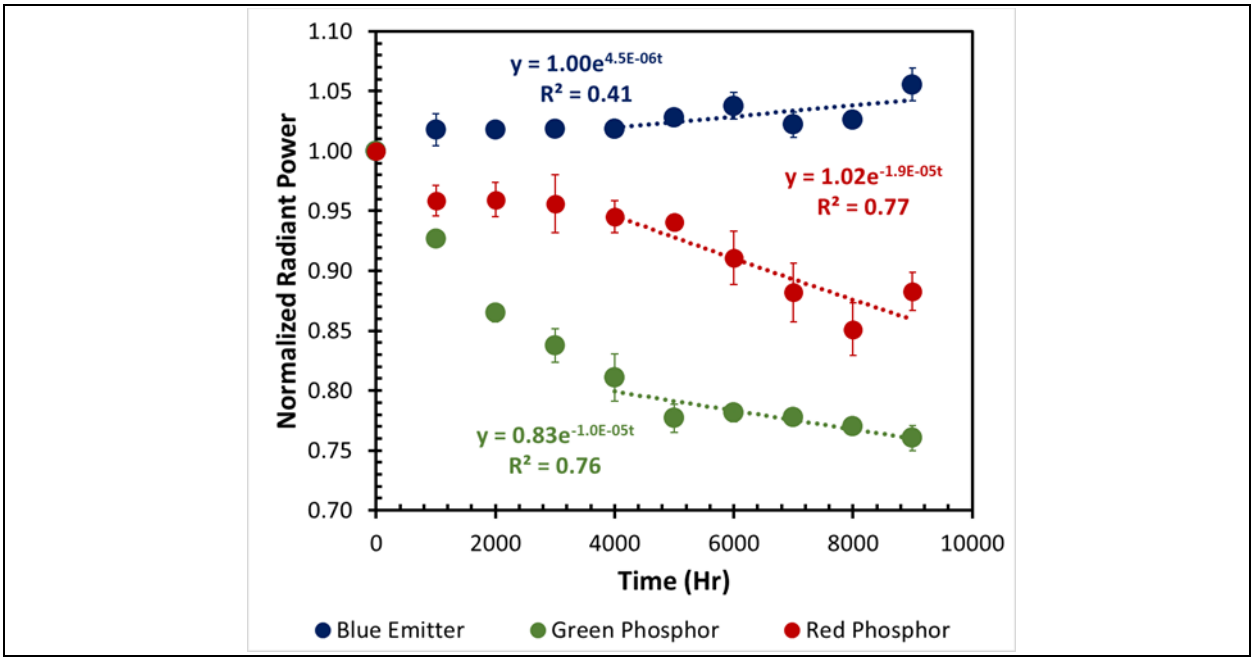

Figure 3-6: The radiant power derived from emission spectra modeling for Product NB-2 exposed to the 7575 test condition.

Table 3-2: Decay rates of the individual emitters in the 7575 test population for Product NB-2.

Emitter	
Blue LEDs	$-4.5 \times 10^{-06} \pm 1.6 \times 10^{-06}$
Green Phosphor	$1.0 \times 10^{-05} \pm 6.9 \times 10^{-06}$
Red Phosphor-QD Mixture	$1.9 \times 10^{-05} \pm 2.5 \times 10^{-06}$

3.3 Product NB-3

3.3.1 Luminous Flux Maintenance

Photometric testing was performed on Product NB-3 after each 1,000 hrs of exposure to the RTOL, 75OL, and 7575 environments in accordance with the ANSI/IES LM-84-20 method [23] to determine LFM values. These products were put into AST much later than Product NB-1 and Product NB-2, so the cumulative hours of exposure are less but have reached the 6,000 hr level for RTOL. Consequently, the results of RTOL testing were analyzed in the same manner as the other NB products by using an exponential decay model as called for in ANSI/IES TM-28-20 [24]. The findings are presented in **Figure 3-7**.

As shown in **Figure 3-7,** Product NB-3 showed practically no luminous flux degradation (LFM > 0.995) after 6,000 hrs of continuous operation in RTOL. The α value measured under these conditions, $3.5x10^{-6}$, is slightly higher than that measured for Product NB-2 in RTOL and likely reflects some uncertainty in the measurement due to the limited test time of NB-3.

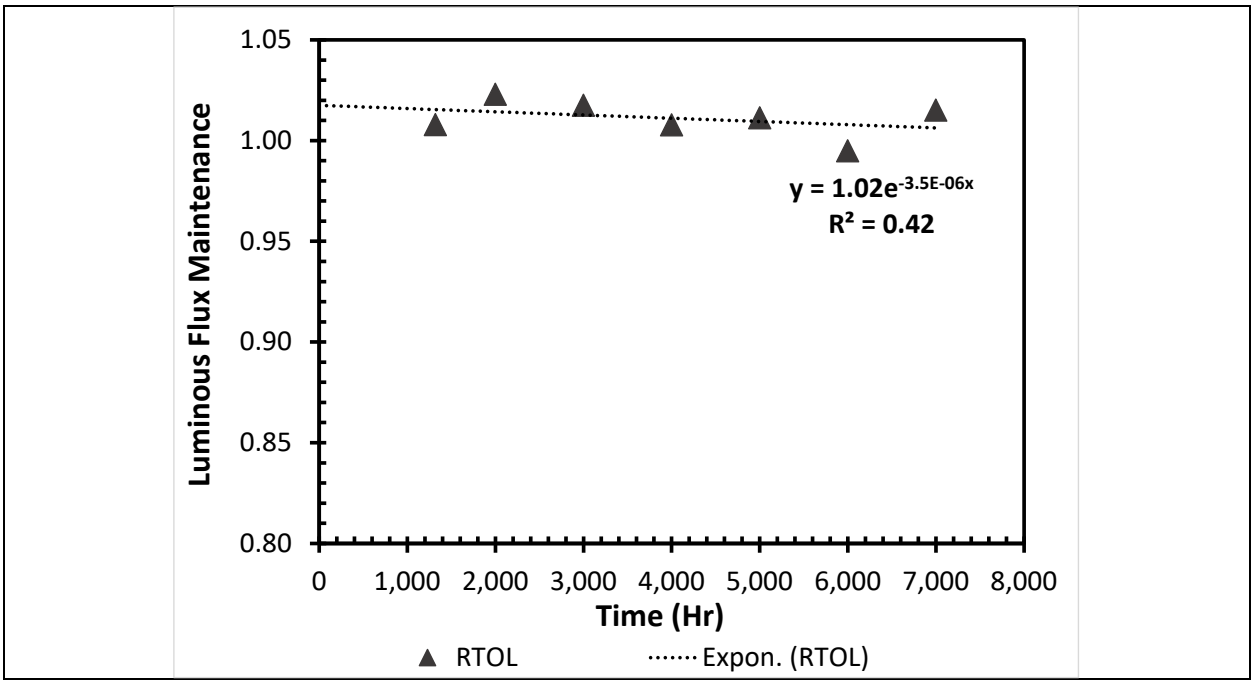

Figure 3-7: LFM of Product NB-3 during RTOL according to ANSI/IES LM-84-20 and ANSI/IES TM-28-20.

3.3.2 Chromaticity Maintenance

The chromaticity shift for the DUTs in RTOL was minimal with $\Delta u'v'$ being less than 0.0006 for all readings through 6,000 hrs of use as shown in **Figure 3-8**.

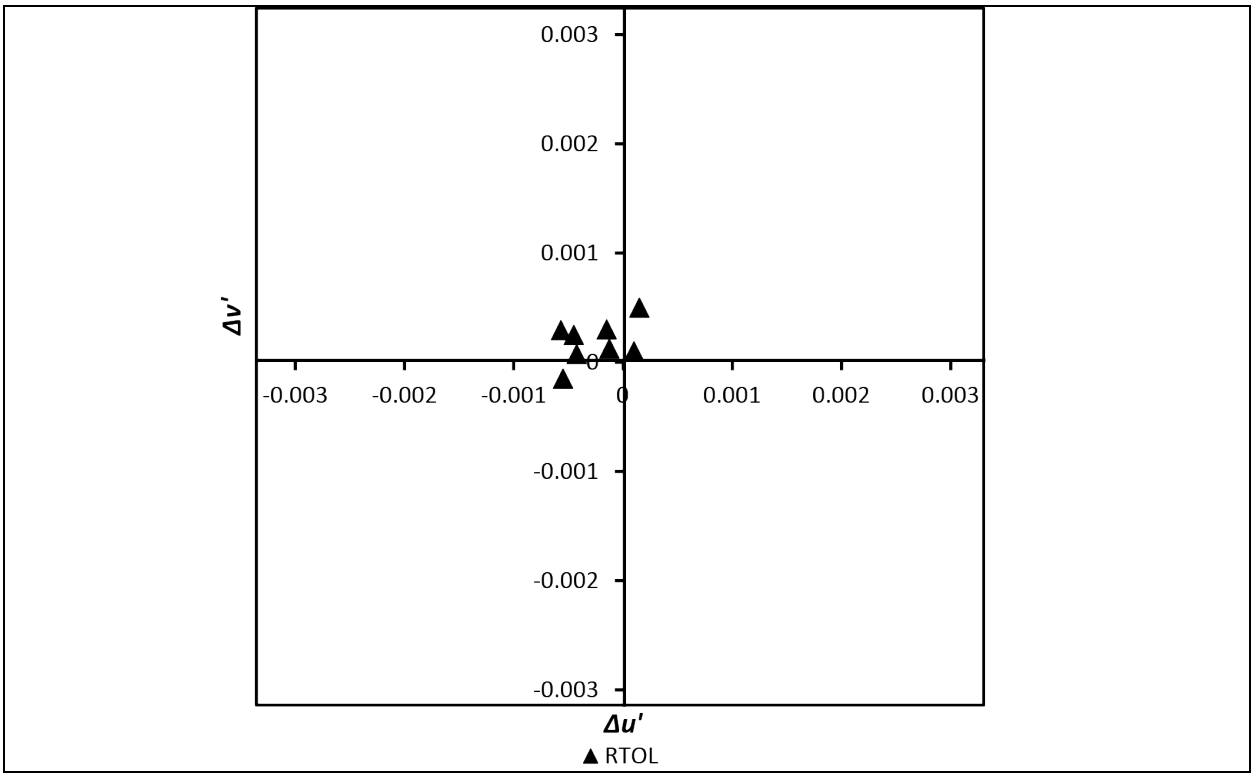

Figure 3-8: Chromaticity shift of Product NB-3 during RTOL.

4 Discussion

4.1 Device Efficiency

The overall efficiency of the DUTs examined in this study depend on many factors such as the efficiency of electrical conversion to blue photons by the LEDs ($\eta_{blue,EQE}$), the efficiency of the conversion of the blue photons to broadband white photons by the secondary converter ($\eta_{phos,EQE}$), the efficiency of light extraction from the LED package, and the efficiency of the human retina to detect the emitted photons (i.e., photopic response). The goal of this report is to compare the LER of SSL products with NB red emitters to that of conventional SSL products with broadband phosphor emitters. However, LER is influenced to some extent by each of these efficiency factors. Therefore, to fully account for LER differences, a comparison of these factors is needed.

4.1.1 Blue LED Efficiency

The EQE of a blue LED ($\eta_{blue,EQE}$) describes the efficiency of blue light emission from the LED into the surrounding medium. It is a product of how efficiently carrier electrons are converted to photons in the LED and the efficiency of extracting these photons from the package. While the efficiency of converting carrier electrons to blue light depends on the properties of the epitaxial layer in the LED, the extraction efficiency depends upon the structure of the LED (e.g., surface roughness, shape) and the index of refraction of the surrounding medium. The index of refraction of gallium nitride (GaN) is high (~ 2.4) whereas that of the silicone is lower (1.45 to 1.55), and the index of refraction of air is lower still at 1.0. Due to the mismatch in index of refraction, you would expect the extraction efficiency of the blue LEDs to be lower in the decapped state (when the GaN is radiating into air and there is more Fresnel reflection at the chip-air interface due to a larger critical angle) than in the silicone covered state. The extent of these differences will vary by package size and type. In addition, the size of the LED die(s) and other potential light-absorbing structures (e.g., bond pads) in the light path may have an impact. As shown in the LED pictures in **Appendix C**, all LED packages

for the products examined in this study are white plastic MP-LED packages of approximately the same size. While the reflectance of each resin was not measured, it can be assumed to be similar. Therefore, we expect that the $\eta_{blue,EQE}$ values measured in this study to be approximations that are directionally correct and can allow comparison, but are not absolute values.

The $\eta_{blue,EQE}$ is defined as the number of photons emitted externally divided by the number of carriers passing the junction (i.e., the number of injected electrons) as shown in Equation 6 [30].

$$\eta_{blue,EQE} = \frac{\text{number of photons emitted externally}}{number\ of\ carriers\ passing\ junction} = \frac{\Phi_e/h\nu}{I/e} \quad \text{(Eq. 5)}$$

In Equation 6, Φ_e is the optical output power, $h\nu$ is the photon energy at the emission frequency ν (h is Planck's constant), I is the injection current, and e is the electron charge. The $\eta_{blue,EQE}$ determined from this analysis are presented in **Table 4-1**. The values typically fall in the range of 0.50 and 0.66 under these conditions.

Table 4-1: EQE of the Blue LEDs

DUT	Estimated $\eta_{blue,EQE}$	I_f (mA, LED Chip)
Product NB-1 (3,500 K)	0.50	96.0
Product NB-2 (2,750 K)	0.61	73.4
Product NB-3[a] (4,000 K)	0.66	73.6
Product MS-4 (2,700 K)	0.57	24.1
Product MS-4 (5,000 K)	0.53	24.3
Product MS-5 (2,700 K)	0.57	169
Product MS-5 (5,000 K)	0.53	169

[a] The power supplied to Product NB-3 was adjusted to make its I_f equivalent to the I_f of Product NB-2 to provide a more direct comparison.

In general, the emitters used in the QD-containing NB products (i.e., Products NB-2 and NB-3) had the highest $\eta_{blue,EQE}$ values ($\eta_{blue,EQE} > 0.6$). The switchable downlights (i.e., Products MS-4 and MS-5) had $\eta_{blue,EQE}$ values similar to each other and lower than the QD-containing products. Product NB-1 had the lowest $\eta_{blue,EQE}$ value (0.50) but also the highest operational current across the blue emitter (96 mA) of the NB products. In addition, Product NB-1 had LED die of two different sizes, and the calculated $\eta_{blue,EQE}$ value is an average of the two. The die size for the LED packages that contained the PFS phosphor (i.e., yellow packages in **Figure A-2**) was smaller than that of the LED packages that had a more conventional nitride phosphor (i.e., orange packages in **Figure A-2**).

4.1.2 Secondary Converter Efficiency

The $\eta_{phos,EQE}$ value of each DUT is the number of photons emitted by the secondary converter divided by the number of photons absorbed by the secondary converter, as shown in Equation 7. For monochromatic radiation of wavelength λ, the photon flux (n) can be calculated from the radiant flux (Φ_e) according to Equation 7.

$$n = photon\ flux\ in\ photons/second = \frac{\lambda \Phi_e}{hc} \quad \text{(Eq. 6)}$$

where h is Planck's constant (6.626 x 10^{-34} J s) and c is the speed of light (3x10^{-8} m/s). If the wavelength (λ) is expressed in nm and Φ_e in watts, this equation can be simplified as shown in Equation 8:

$$n = photon\ flux\ in\ photons/second = (5.03\ x\ 10^{15})\lambda \Phi_e \quad \text{(Eq. 7)}$$

For an SPD containing non-monochromatic light (e.g., white light), the centroid wavelength of phosphor emissions ($\bar{\lambda}_{phos}$) and the radiant flux of phosphor emissions ($\Phi_{e,phos}$) can be used to provide the number of photons in the emitted white light as shown in Equation 9.

$$n = photon\ flux\ in\ photons/second = (5.03\ x\ 10^{15})\bar{\lambda}_{phos}\Phi_{e,phos} \quad \text{(Eq. 8)}$$

To calculate $\eta_{phos,EQE}$, the amount of blue light absorbed by the phosphor must be determined. This value can be approximated as the difference between the blue light emissions of the decapped LED ($\Phi_{e.blue}$) and the blue light content of the white spectrum produced by the LED ($\Phi_{e.bluewhite}$). The value is only an approximation given the change in index of refraction between the normal and decapped LEDs. As a result, the quantum efficiency calculated in this manner will be higher than the true quantum efficiency. These values are not the absolute quantum efficiency, but more of a relative quantum efficiency value that should be directionally correct to allow comparisons. Under these assumptions, the quantum efficiency can be calculated using Equation 10:

$$\eta_{phos,EQE} = \frac{\bar{\lambda}_{phos}\Phi_{e,phos}}{\bar{\lambda}_{\text{blue}}(\Phi_{e,blue} - \Phi_{e,bluewhite})} \quad \text{(Eq. 9)}$$

Several assumptions underlie the calculation of quantum efficiency in this manner, so it is best to compare similar products. Comparisons between dissimilar products should be avoided. Since Product NB-2 and NB-3 contain LEDs from the same manufacturer's product family, the results from these two products can be compared. As shown in **Table 4-2,** the initial phosphor quantum efficiency of Product NB-3 is higher than that of Product NB-2. This finding may be due to the higher concentration of red secondary converters (e.g., quantum dots) in Product NB-2, which can be expected to have a lower efficiency. The higher concentration of red secondary converters is necessary to achieve the warmer CCT value. A similar decrease in quantum efficiency was observed for Product MS-4 and Product MS-5 as the CCT value decreased. The estimated $\eta_{phos,EQE}$ for Product NB-1 was the highest, but caution is urged in interpreting this value because it is not an absolute quantum efficiency.

Table 4-2: EQE of the Secondary Emitters

Label	Approximate Value of $\eta_{phos,EQE}$
Product NB-1 (3,500 K)	0.99
Product NB-2 (2,700 K)	0.89
Product NB-3 (4,000 K)	0.97
Product MS-4 (2,700 K)	0.95
Product MS-4 (3,500 K)	0.97
Product MS-4 (4,000 K)	0.98
Product MS-5 (2,700 K)	0.87
Product MS-5 (3,500 K)	0.87
Product MS-5 (4,000 K)	0.91

4.2 Impact of Device Efficiencies on Radiant Efficiency and LER

In our previous report, we examined the spectral efficiency of Products NB-1 and NB-2 and compared the LER of these products to Product MS-4, a downlight that has conventional pc-LEDs and the ability to be tuned to five CCT settings between 2,700 K and 5,000 K. In this report, we extend this comparison to Product MS-5 (another switchable downlight that uses conventional pc-LEDs, see **Section 2.1.5**) and provide initial benchmarks for Product NB-3. The efficiency parameters of these products are shown in **Table 4-3.**

Table 4-3: Efficiency Parameters

DUT (nominal CCT)	Power to LED Module (W)	Radiant Flux (W)	Device Radiant Efficiency (%)	Luminous Flux (lm)	LER (lm/W)
Product NB-1 (3,500 K)	8.98	4.03	44.9	1,326	329
Product NB-2 (2,750 K)	10.23	4.04	39.5	1,188	294
Product NB-3 (4,000 K)	23.87	12.64	53.0	3,923	310
Product MS-4 (2,700 K)	7.51	2.95	39.2	842	285
Product MS-4 (3,500 K)	6.15	3.06	49.8	870	284
Product MS-4 (4,000 K)	6.35	3.11	49.0	882	284
Product MS-5 (2,700 K)	10.37	3.57	34.4	1,041	292
Product MS-5 (3,500 K)	8.52	3.68	43.2	1,063	289
Product MS-5 (4,000 K)	8.66	3.77	43.5	1,089	289

In interpreting **Table 4-3**, it is critical to understand the difference between device radiant efficiency and LER. Radiant efficiency can be defined as the ratio of the radiant flux of emitted radiation produced by a device to the input electrical power consumed by the source to produce that radiation [3]. In contrast, LER is defined as the quotient of the total luminous flux divided by the total radiant flux produced by the device [3]. Both of these measurements are absolute values of the lighting system derived from integrating sphere measurements calibrated to NIST standards. Radiant efficiency is more of a measure of the overall performance of the devices and is impacted by both $\eta_{blue,EQE}$ and $\eta_{phos,\mathrm{EQE}}$, but is not affected by spectral match with the photopic sensitivity curve. In contrast, LER measures how efficiently blue photons are converted to radiation that matches the sensitivity of the human retina (i.e., photopic sensitivity). Consequently, LER is dependent upon both $\eta_{phos,\mathrm{EQE}}$ and the photopic sensitivity curve.

Product NB-1 exhibited the highest LER value measured in this study, which can be attributed to a combination of the high relative quantum efficiency of this product (See **Table 4-2**) and the match of the spectral radiation with the photopic sensitivity curve. However, the radiant efficiency of the device fell between the values for the two conventional SSL benchmark products (MS-4 and MS-5). We attribute this finding to the relatively low value of $\eta_{blue,\mathrm{EQE}}$ estimated for this product (see **Table 4-1**). Using an emitter with a higher $\eta_{blue,\mathrm{EQE}}$ would likely provide a product that delivers both high LER and high radiant efficiency.

Product NB-2 exhibited improved radiant efficiency and LER over both convention LED products at the same CCT value, but likely for different reasons. The differences in performance between Products NB-2 and MS-4 at 2,700 K are small. The radiant efficiencies are almost the same, but the LER of Product NB-2 is higher, likely reflecting an improved match between the emission spectrum and the photopic sensitivity curve provided by the use of the narrow-band red QD secondary converter. The radiant efficiency of Product NB-2 is significantly higher than that of Product MS-5 at 2,700 K, possibly due to the higher $\eta_{blue,\mathrm{EQE}}$ of the narrow-band product.

For Product NB-3, the combination of higher relative $\eta_{blue,\mathrm{EQE}}$ and $\eta_{phos,\mathrm{EQE}}$ led to advantages in both radiant efficiency and LER over conventional SSL phosphor products (i.e., Products MS-4 and MS-5) at the same CCT value. However, the benefits of these gains are dampened unless the emitted spectrum contains light at

the wavelengths of retina response. Fortunately, Product NB-3 has an excellent match to the photopic sensitivity curve as shown by its high LER value (310 lm/W).

There is a clear dependence of radiant efficiency on nominal CCT values as demonstrated by both conventional SSL products (Products MS-4 and MS-5). Higher CCT values tend to have higher radiant efficiencies most likely due to the rise in $\eta_{phos,\mathrm{EQE}}$ as CCT values increase and fewer red emissions are required in the spectrum. For the NB products, the lower relative value of $\eta_{blue,\mathrm{EQE}}$ estimated for Product NB-1 resulted in a lower radiant efficiency than the other products, although this device had the best relative $\eta_{phos,\mathrm{EQE}}$ value and LER. The use of an improved LED emitter would likely boost the radiant efficiency of the system.

These findings provide comparisons between the radiant efficiency and LERs of the NB products with SSL products containing conventional nitride phosphors that are broadband emitters. Clearly, the use of NB red emitters can improve LER by as much as 15% over conventional SSL products. These high LER values can be achieved simultaneously with excellent color rendering, demonstrating that both efficiency and good color rendering can be achieved in the same product. When combined with high efficiency LED emitters, these NB technologies will provide a superior illumination source that combines both high radiant efficiency and high LER into the same product.

5 Conclusions

Achieving high LER performance, radiant efficiency, and good color rendering in SSL sources is complicated by the inherent trade-offs between NB sources (which generally promote high LER) and broadband sources (which generally promote high color rendering). This report examines three NB red emitter technologies that balance these trade-offs and achieve improved performance over conventional SSL technologies that employ nitride phosphors that emit broadly in the red. The products examined in this study are labeled NB-1, NB-2, and NB-3 for narrow-band red products and MS-4 and MS-5 for multi-spectrum products that used conventional SSL phosphor technologies. All products had excellent color rendering properties ($R_f \geq 93$, $R_g = 99$). Product NB-1 utilized manganese-doped PFS phosphors that produce NB emissions at five distinct bands between 609 nm and 648 nm. Product NB-1 exhibited the highest LER (329 lm/W) and phosphor EQE of the devices tested. Products NB-2 and NB-3 both used QD-phosphor secondary converters to provide red emissions in a peak at approximately 620 nm that is narrower than the emission peak nitride red-emitting phosphors used in many SSL devices. This approach allowed Products NB-2 and NB-3 to achieve LER values between 294 and 310 lm/W depending on the CCT of the device while also exhibiting excellent radiant efficiencies. The lifetime performance of Products NB-1 and NB-2 were examined through AST protocols in 75OL and 7575 environments. The findings from this testing demonstrated that Products NB-1 and NB-2 performed nearly as well at elevated ambient temperatures (75°C) as they do at room temperature. However, exposure to environments with elevated temperature and humidity (e.g., 75° C and 75% humidity) accelerated the decay of luminous flux maintenance and caused significant chromaticity shifts. These findings provide a guide for the use of NB red emitter technologies in SSL applications and demonstrate that excellent performance can be achieved with both PFS and QD NB technologies in normal indoor environments.

References

1. Hodapp, M.W. (1997). Applications of high-brightness light-emitting diodes. Pp. 227-356 in G.B. Stringfellow and M.G. Craford (eds.), *Semiconductors and Semimetals*, vol. 48, R.K. Willardson and E.R. Weber (series eds.), New York: Academic Press.

2. Smallwood, P. (2018). *Global LED and lighting market overview*. Presentation at 2018 Strategies in Light, Long Beach, CA.

3. ANSI/IES LS-1-20. (2020). *Lighting Science: Nomenclature and Definitions for Illuminating Engineering*. Available at https://www.ies.org/standards/definitions/.

4. ANSI (American National Standards Institute) and IES (Illuminating Engineering Society) (2020). *ANSI/IES TM-30-20: IES Method for Evaluating Light Source Color Rendition.* New York, NY: IES.

5. Naab, D., Murphy, J. (2019). *GE K2Si4:Mn4+ (PFS/KFS) phosphor: Market leading wide color gamut technology and path towards enable next generation displays*. Presentation at 2019 Meeting of the Society for Information Display (SID). San Jose, CA.

6. Radkov, E.V., Grigorov, L.S., Setlur, A.A., Srivastava, A.M. (2009). U.S. Patent 7,497,973. Red line emitting phosphor materials for use in LED applications.

7. European Commission. (2011). *Restriction of Hazardous Substances in Electrical and Electronic Equipment*. Information available at https://ec.europa.eu/environment/topics/waste-and-recycling/rohs-directive_en.

8. Poole, C.P. Jr., Owens, F.J. (2003). *Introduction to Nanotechnology,* Hoboken, NJ: Wiley.

9. Mutavdzic, D., Xu, J., Thakur, G., Triulzi, R., Kasas, S., Jeremic, M., Leblanc, R., Radotic, K. (2011) Determination of the size of quantum dots by fluorescence spectroscopy. *Analyst*, 136(11), 2391–2396.

10. Davis, J. L. and Mills, K.C. (2010). *Photoluminescent nanofibers for high efficiency solid-state lighting.* Final report on DOE Project DE-FC26-06NT42861 submitted to the U.S. Department of Energy.

11. Shimizu, K.T., Bohmer, M., Estrada, D., Gangwal, S., Brabowski, S., Bechtel, H., Kang, E., Vampola, K.J., Chamberlin, D., Shchekin, O.B., Bhardwaj, J. (2018). Toward commercial realization of quantum dot based white light-emitting diodes for generation illumination. *Photonics Research,* 5(2), A1–A6.

12. Mangum, B.D., Landes, T.S., Theobald, B.R., Kurtin, J.N. (2018). Exploring the bounds of narrow-band quantum dot downconverted LEDs. *Photonics Research,* 5(2), A13–A22.

13. Owen, J.S., Kurtin, J., Chan, E. (2020). *Environmentally robust quantum dot down converters for high efficiency solid state lighting*. Presentation at the 2020 DOE/IES Lighting Research and Development Workshop, San Diego, CA. Available at https://www.energy.gov/sites/default/files/2020/02/f71/ssl-rd2020-owen-qd_0.pdf.

14. Rreza, I., Yang, H., Hamachi, L., Campos, M., Hull, T., Treadway, J., Kurtin, J., Chan, E.M., Owen, J.S. (2021). Performance of spherical quantum well down converters in solid state lighting. *ACS Applied Materials & Interfaces,* 13, 12191–12197.

15. Kurtin, J., Theobald, B., Carillo, M.J., Park, O.-H., Masson, G., Hughes, S.M. (2016). U.S. Patent 10.074,780. Composite having semiconductor structures including a nanocrystalline core and shell.

16. Rountree, K., Davis, J.L., McCombs, M., Mills, K., Pope, R. (2020). *Initial benchmarks and long-term performance of narrow-band red emitters used in SSL devices*. U.S. Department of Energy, Washington, DC. Available at https://www.energy.gov/sites/default/files/2020/10/f79/ssl-rti-red-emitters-aug2020.pdf.

17. Davis, L., Rountree, K., McCombs, M., Mills, K., Pope, R. (2020). *Changes in SSL Device Efficiency and Optical Performance Under Accelerated Aging Conditions.* U.S. Department of Energy, Washington, DC. Available at https://www.energy.gov/sites/prod/files/2020/08/f77/ssl-rti-device-efficiency-jun2020.pdf.

18. Davis, L., Rountree, K., Mills, K., Pope, R., McCombs, M., Hegarty-Craver, M. (2021). *Changes in SSL Device Efficiency and Optical Performance with Aging: Final Report.* U.S. Department of Energy, Washington, DC.

19. ANSI (American National Standards Institute) and IES (Illuminating Engineering Society) (2019). *ANSI/IES LM-79-19: Approved Method: Optical and Electrical Measurements of Solid-State Lighting Products*. New York, NY: IES.

20. Fraser, R.D.B., Suzuki, E. (1969). Resolution of overlapping bands. Functions for simulating band shapes. *Analytical Chemistry,* 41, 37–39.

21. Reifegerste, F., Lienig, J. (2008). Modelling of the temperature and current dependence of LED spectra. *Journal of Light & Visual Environments*, 32, 288–294.

22. Jeong, S.S., Ko, J.-H. (2012). Analysis of the spectral characteristics of white light-emitting diodes under various thermal environments. *Journal of Information Display*, 13(1), 37-42.

23. IES (Illuminating Engineering Society). (2014). *ANSI/IES LM-84-20: Measuring Luminous Flux and Color Maintenance of LED Lamps, Light Engines, and Luminaires.* New York, NY: IES.

24. ANSI (American National Standards Institute) and IES (Illuminating Engineering Society) (2020). *ANSI/IES TM-28-20: Projecting Long-Term Luminous Flux Maintenance of LED Lamps and Luminaires.* New York, NY: IES.

25. Davis, J.L., Young. J., Royer M. (2016, February). *CALiPER Report 20.5: Chromaticity shift modes of LED PAR38 lamps operated in steady-state conditions.* Available at https://www.energy.gov/sites/prod/files/2016/03/f30/caliper_20-5_par38.pdf.

26. Next Generation Lighting Industry Alliance and the LED (Light-Emitting Diodes) Systems Reliability Consortium. (2017, April). *LED luminaire reliability: Impact of color shift*. Available at https://www.nglia.org/pdfs/lsrc_colorshift_apr2017r.pdf.

27. Nazzal, A.Y., Wang, X., Qu, L., Wu, W., Wang, Y., Peng, X. Xiao, M. (2004). Environmental effects on photoluminescence of highly luminescent CdSe and CdSe/ZnS Core/shell nanocrystals in polymer thin films. *Journal of Physical Chemistry B,* 108(8), 5507–5515. https://doi.org/10.1021/jp035361q

28. Choi, J., Choi, M. J., Kim, J., Dinic, F., Todorovic, P., Sun, B., . . ., Sargent, E. H. (2020). Stabilizing surface passivation enables stable operation of colloidal quantum dot photovoltaic devices at maximum power point in an air ambient. *Advanced Materials, 32*(7), e1906497. https://doi.org/10.1002/adma.201906497

29. Lai, C.-F., Tien, Y.-C., Tong, H.-C., Zhong, C.-Z., Lee, Y.-C. (2018). High-performance quantum dot light-emitting diodes using chip-scale package structures with high reliability and wide color gamut for backlight displays. *RSC Advances,* 8(63), 35966–35972. https://doi.org/10.1039/C8RA07928E

30. Sze, S.M., Ng, K.K. (2006). LEDs and lasers. *Physics of Semiconductor Devices,* pp. 599–662. Hoboken, NJ: Wiley. doi:10.1002/9780470068328.ch12

Appendix A

Figure A-1: Product NB-1 in a traditional fluorescent lighting fixture. The LED tube is 2 ft long.

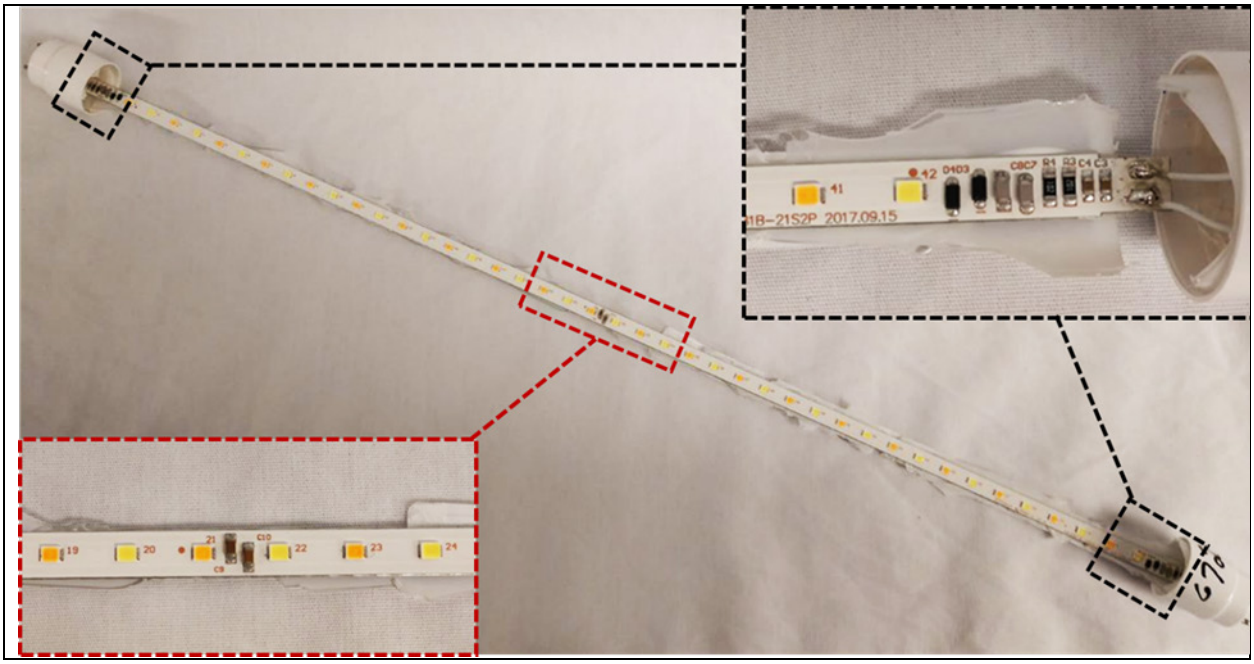

Figure A-2: Product NB-1 with the glass globe removed. The black dotted inset shows the electronic circuitry on the PCB while the red dotted inset shows the arrangement of the LEDs and capacitors in the center of the LED module.

Figure A-3: Product NB-2 LED light engine consisting of two LED modules mounted on a common heat sink. Each LED module is 1 ft long.

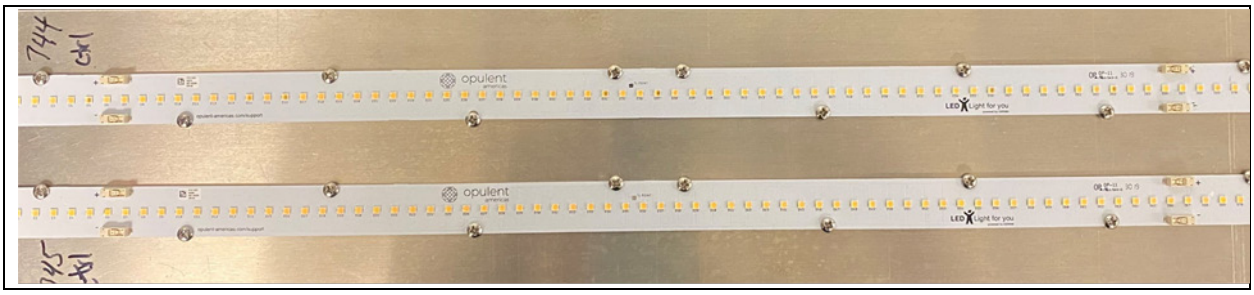

Figure A-4: Product NB-3 LED light engine consisting of two LED modules mounted on a common heat sink. Each LED module is 2 ft long.

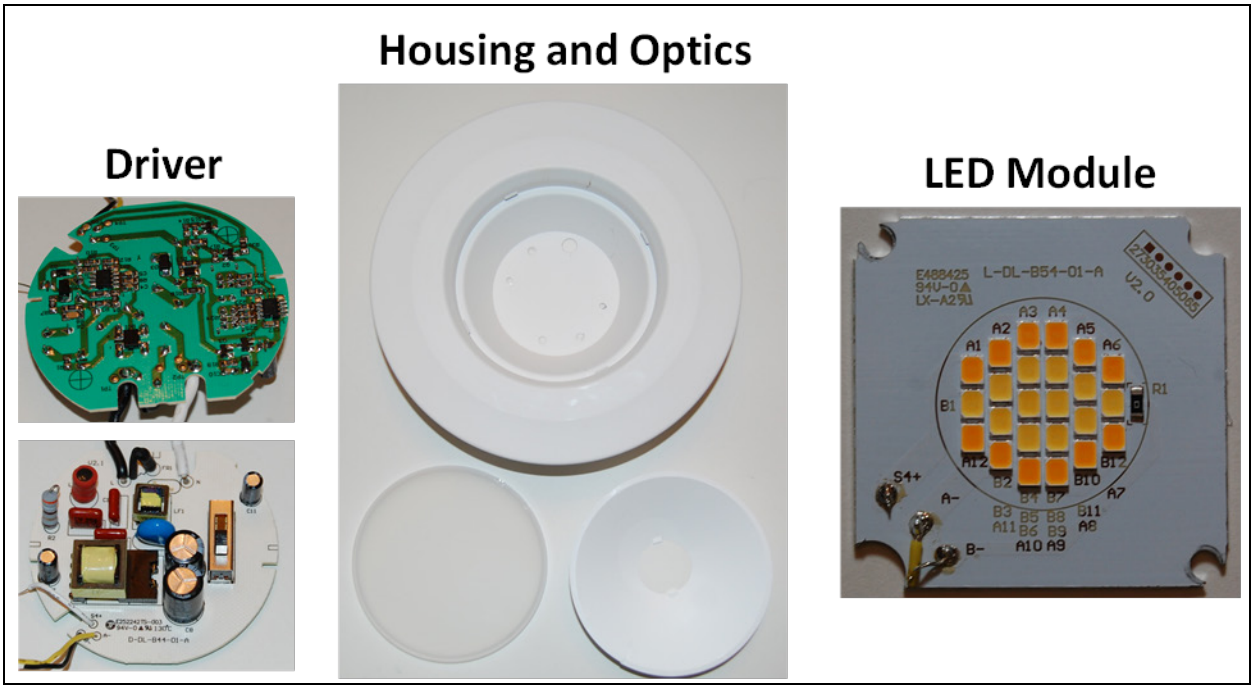

Figure A-5: The components of Product MS-4.

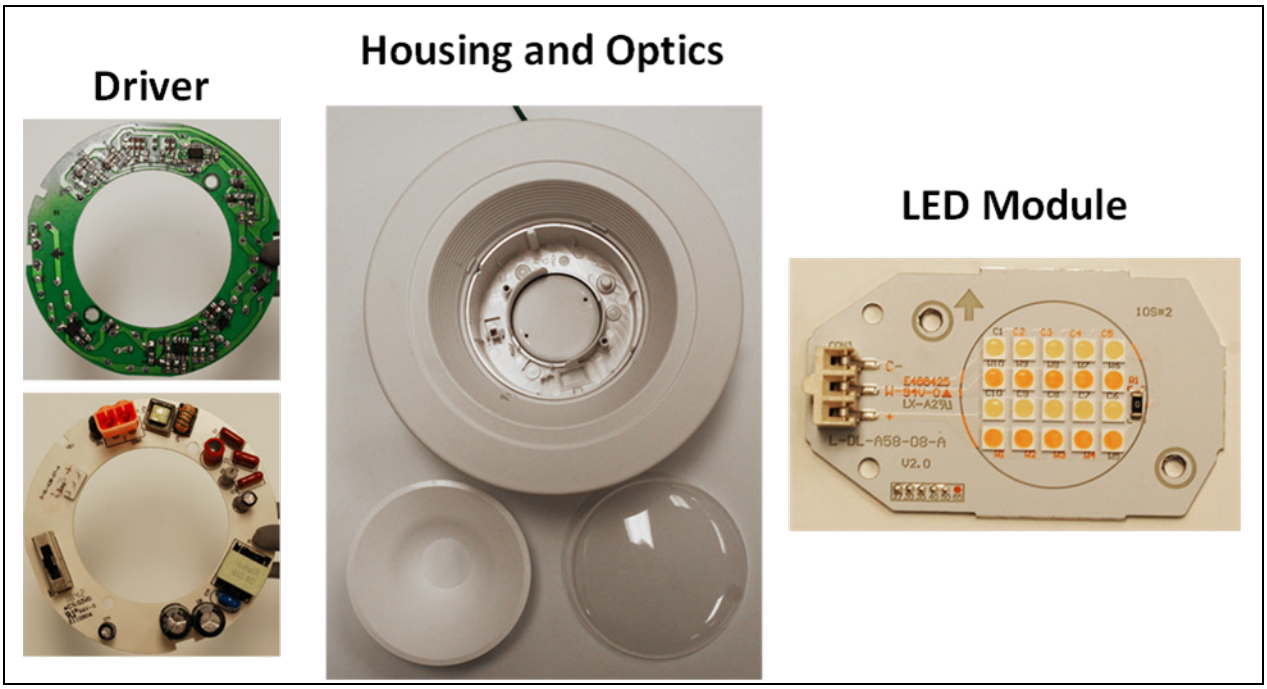

Figure A-6: The components of Product MS-5.

Appendix B

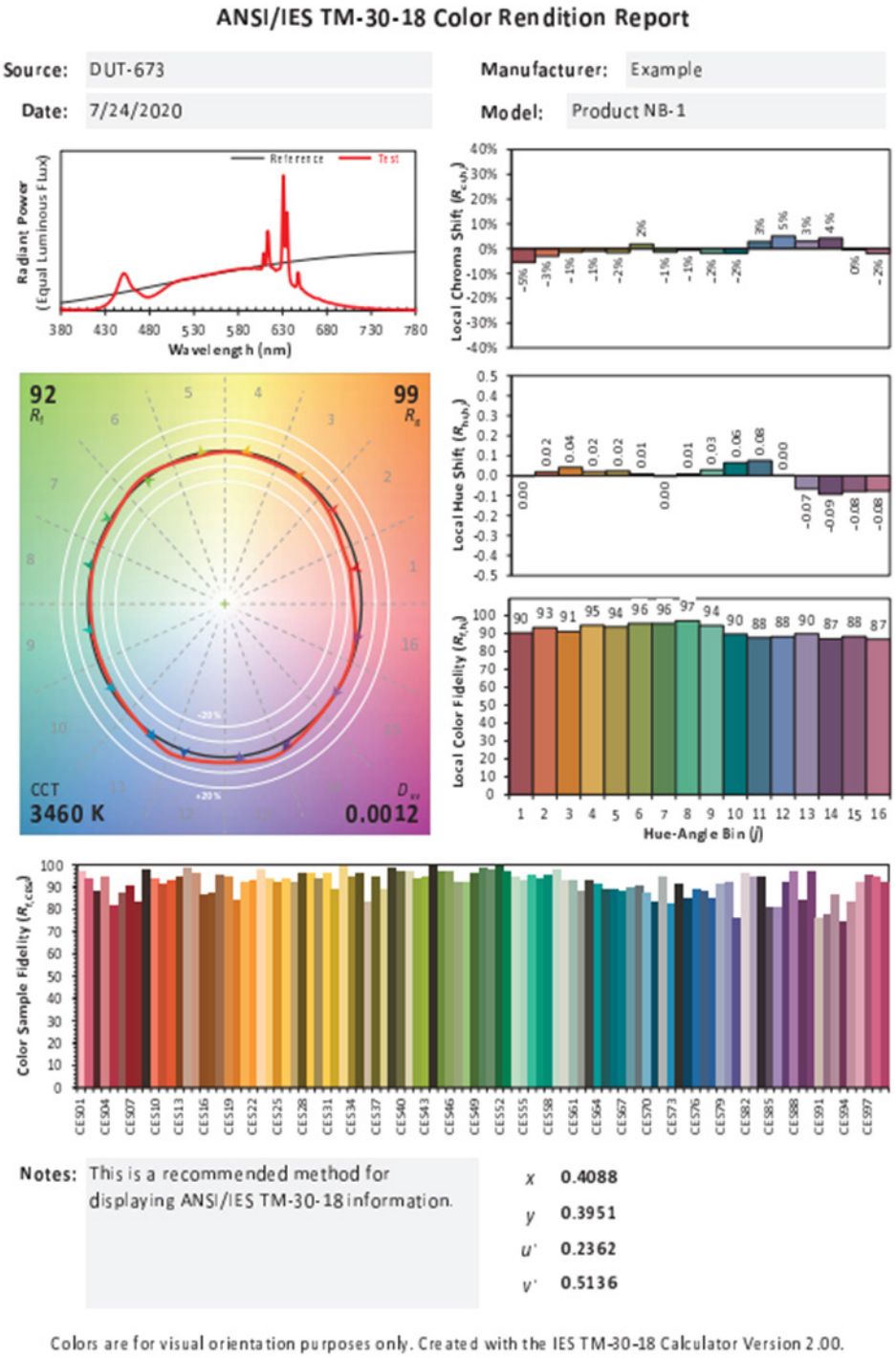

Figure B-1: ANSI/IES TM-30-18 analysis for Product NB-1.

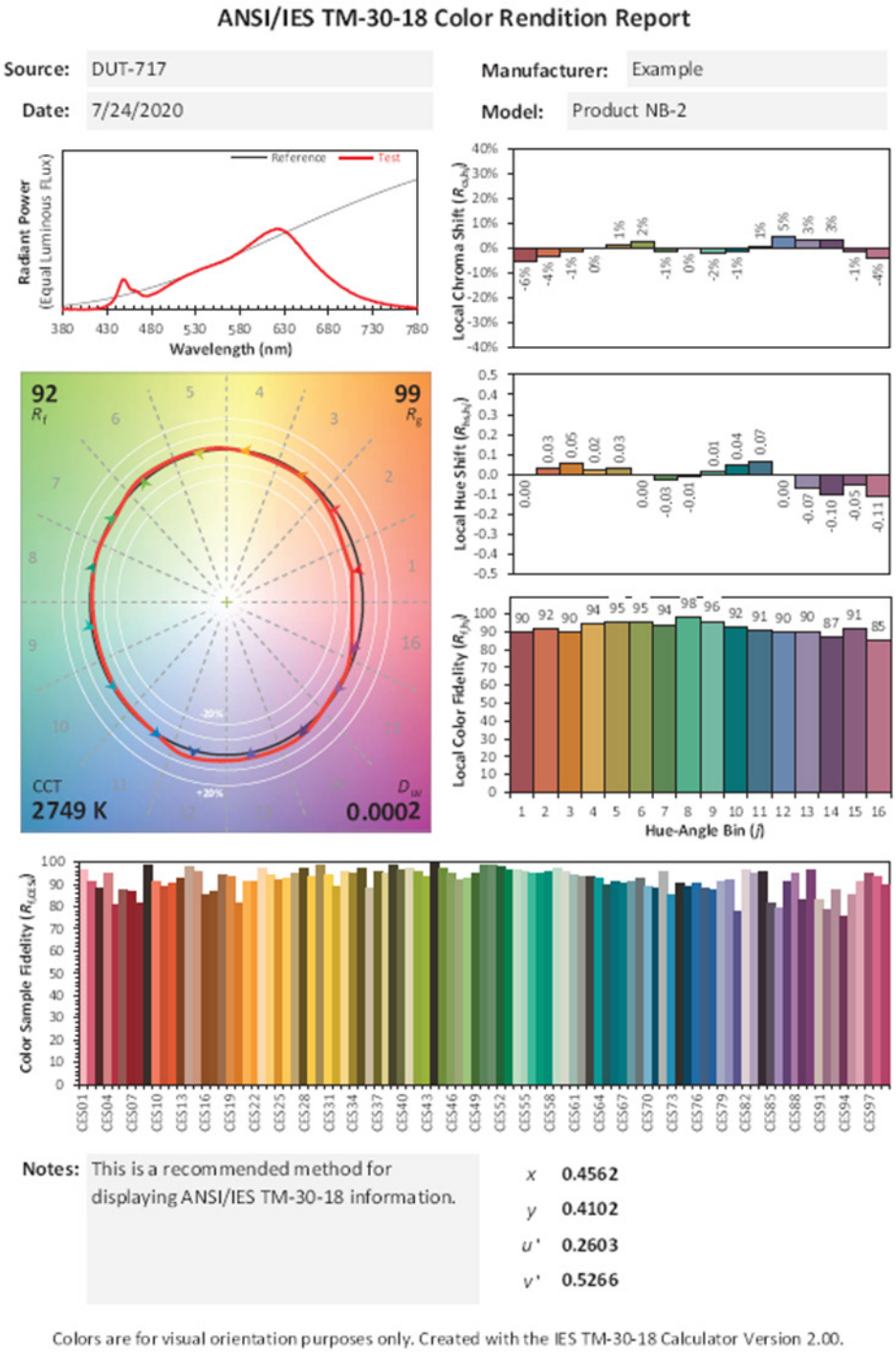

Figure B-2: ANSI/IES TM-30-18 analysis for LEDs from Product NB-2.

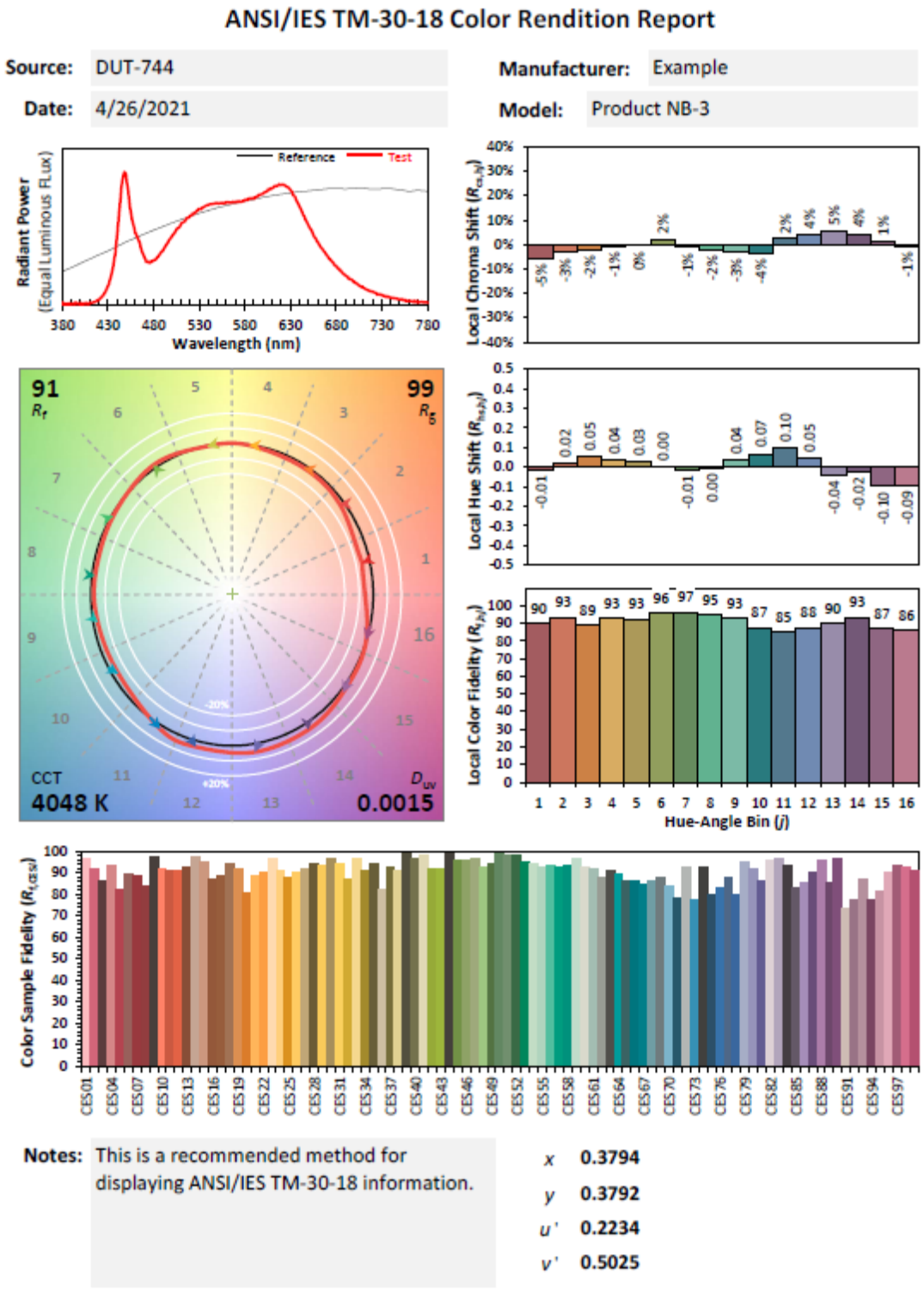

Figure B-3: ANSI/IES TM-30-18 analysis for LEDs from Product NB-3.

Appendix C

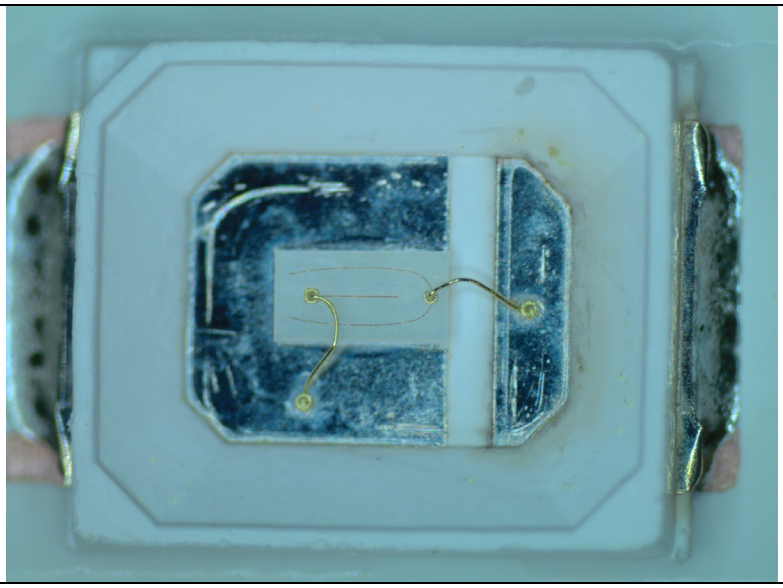

Figure C-1: Microscopy image of a LED package with PFS phosphor from Product NB-1.

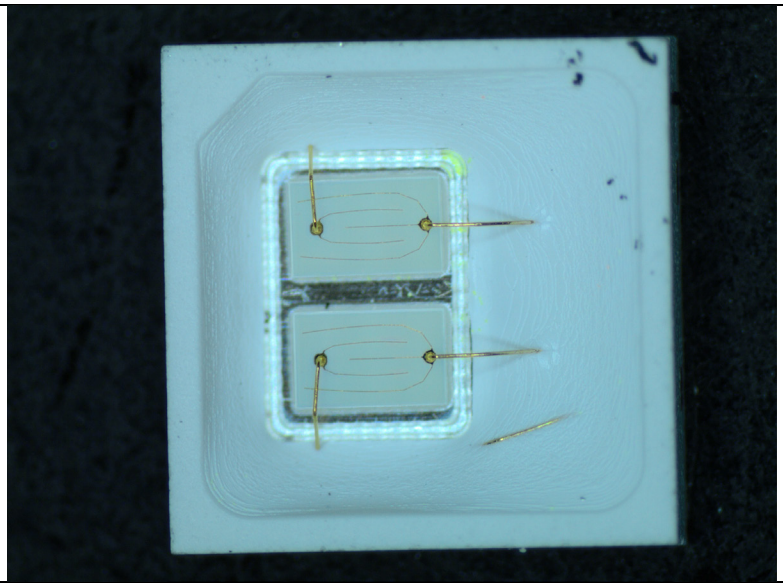

Figure C-2: Microscopy image of an LED package from Product NB-2.

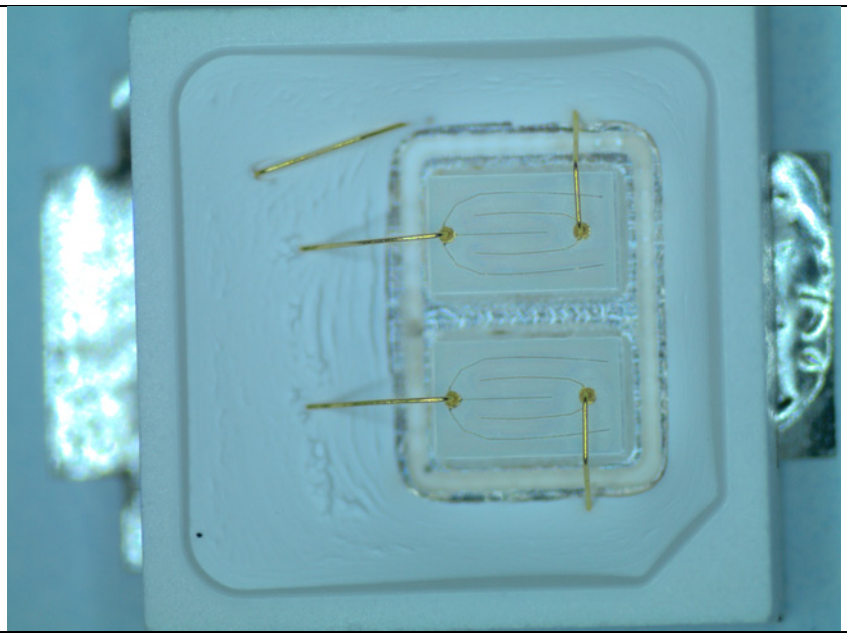

Figure C-3: Microscopy image of an LED package from Product NB-3.

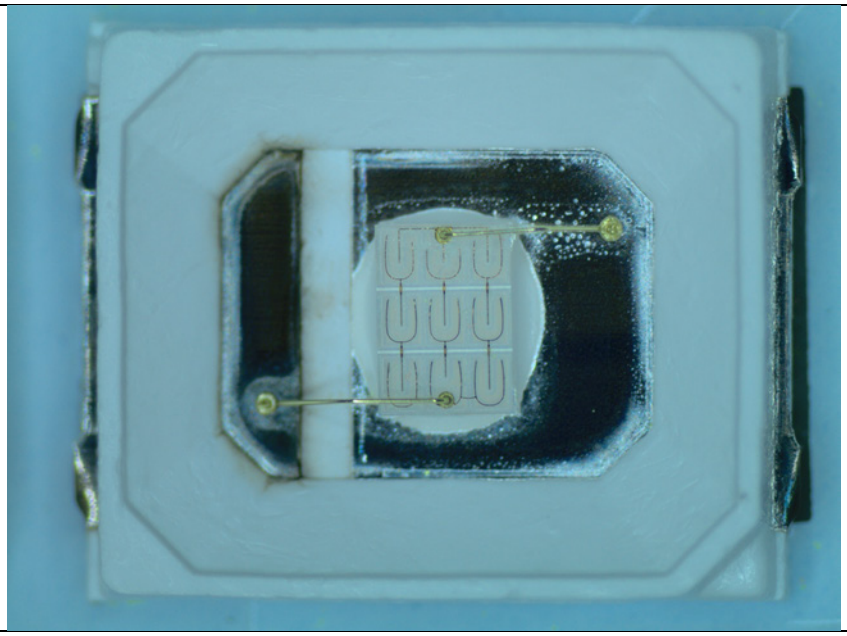

Figure C-4: Microscopy image of an LED package from Product MS-4.

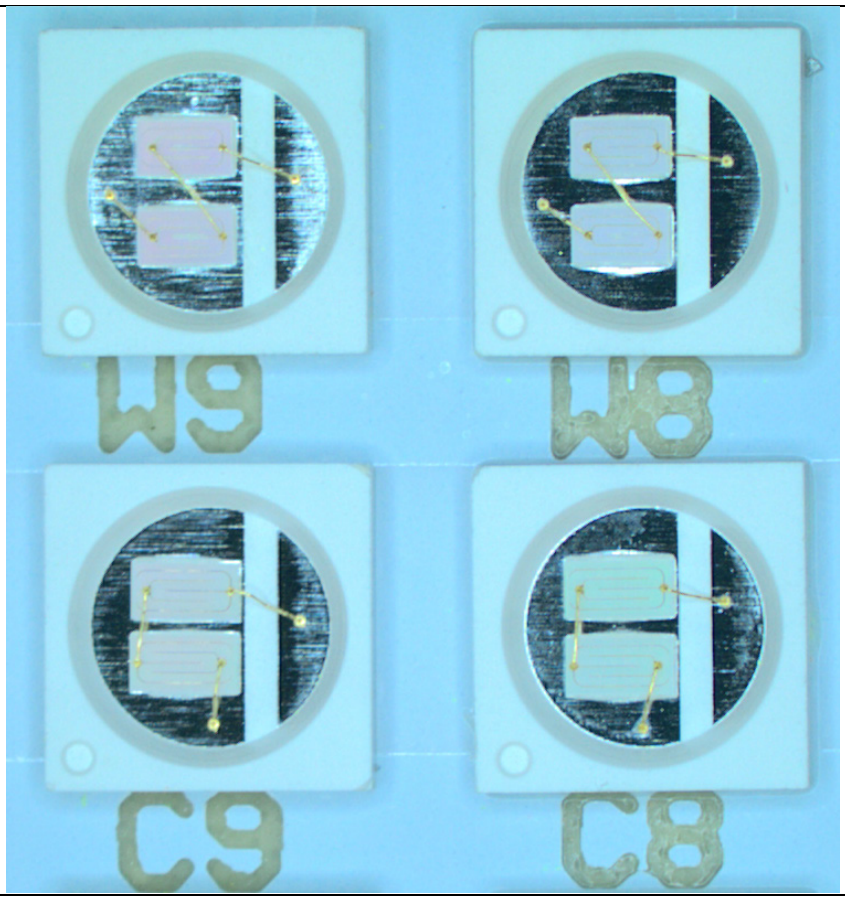

Figure C-5: Microscopy image of LED packages from Product MS-5.

Appendix D

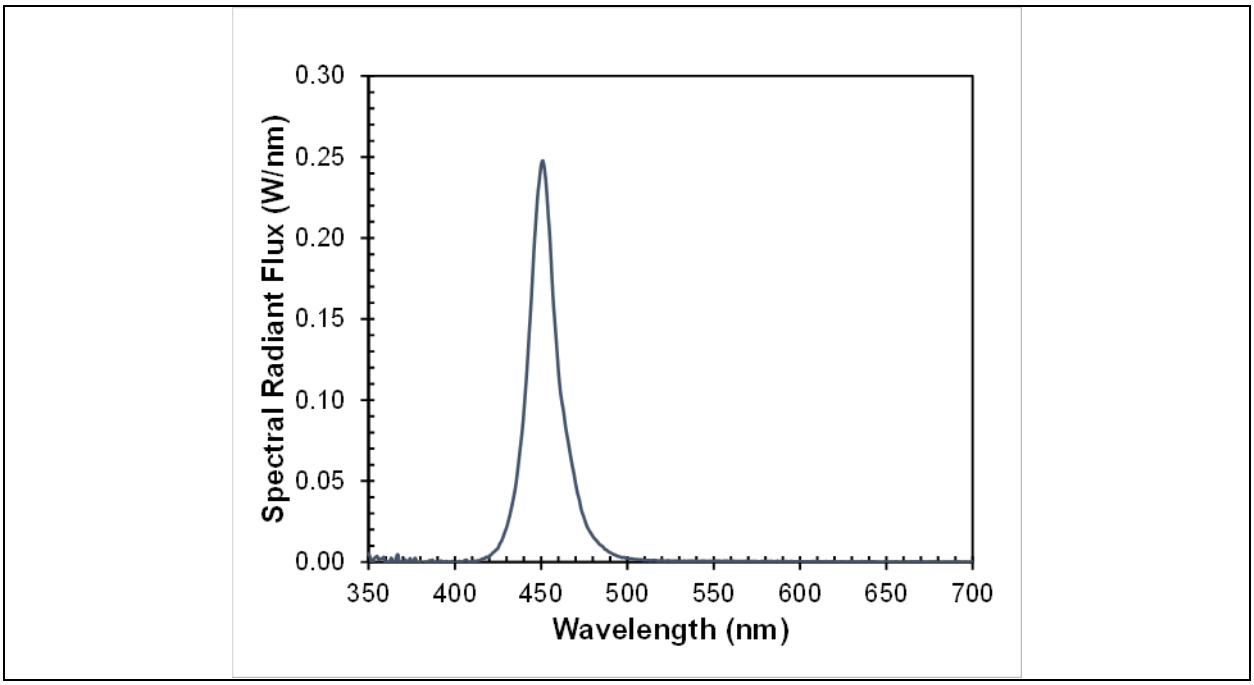

Figure D-1: SPD of Product NB-1 after phosphor removal by decapping.

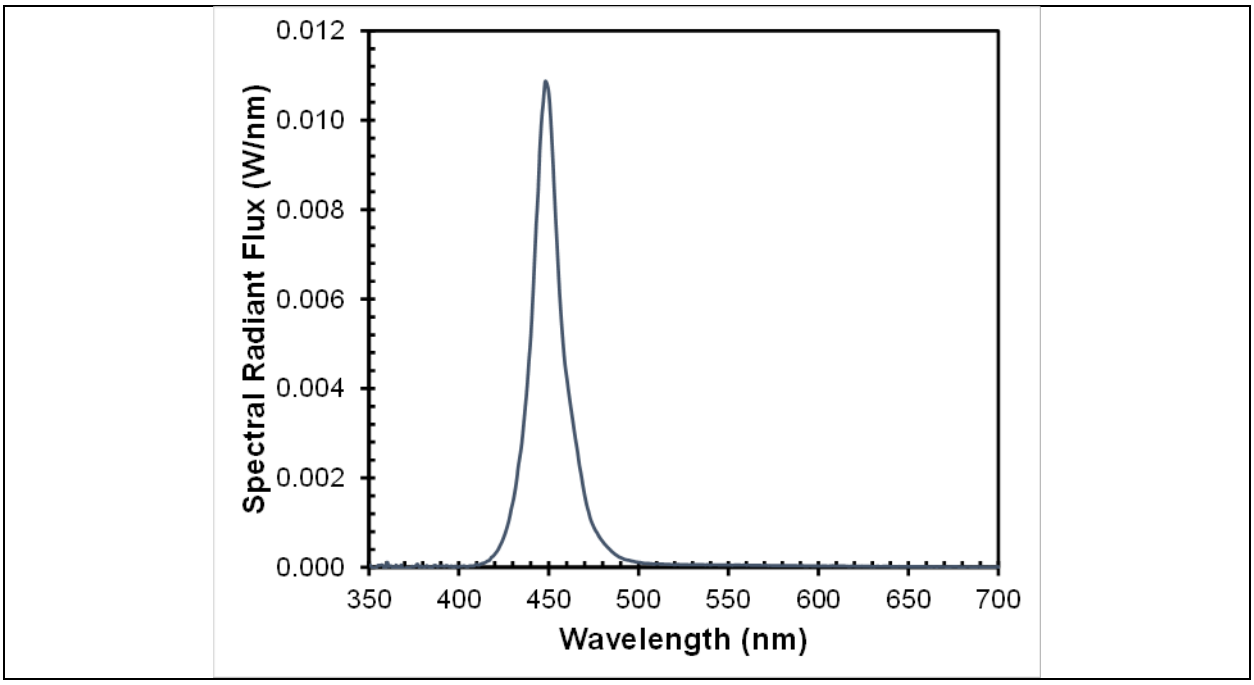

Figure D-2: SPD of a single LED package used in Product NB-2 after phosphor removal by decapping.

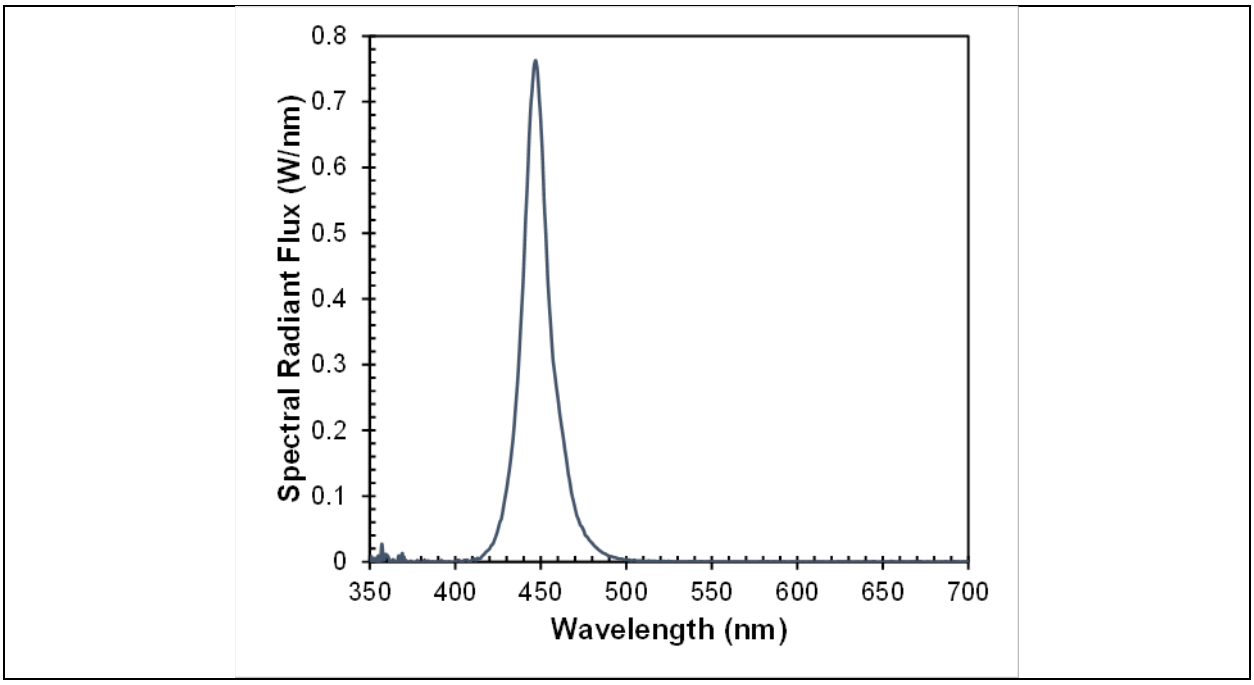

Figure D-3: SPD of Product NB-3 after phosphor removal by decapping.

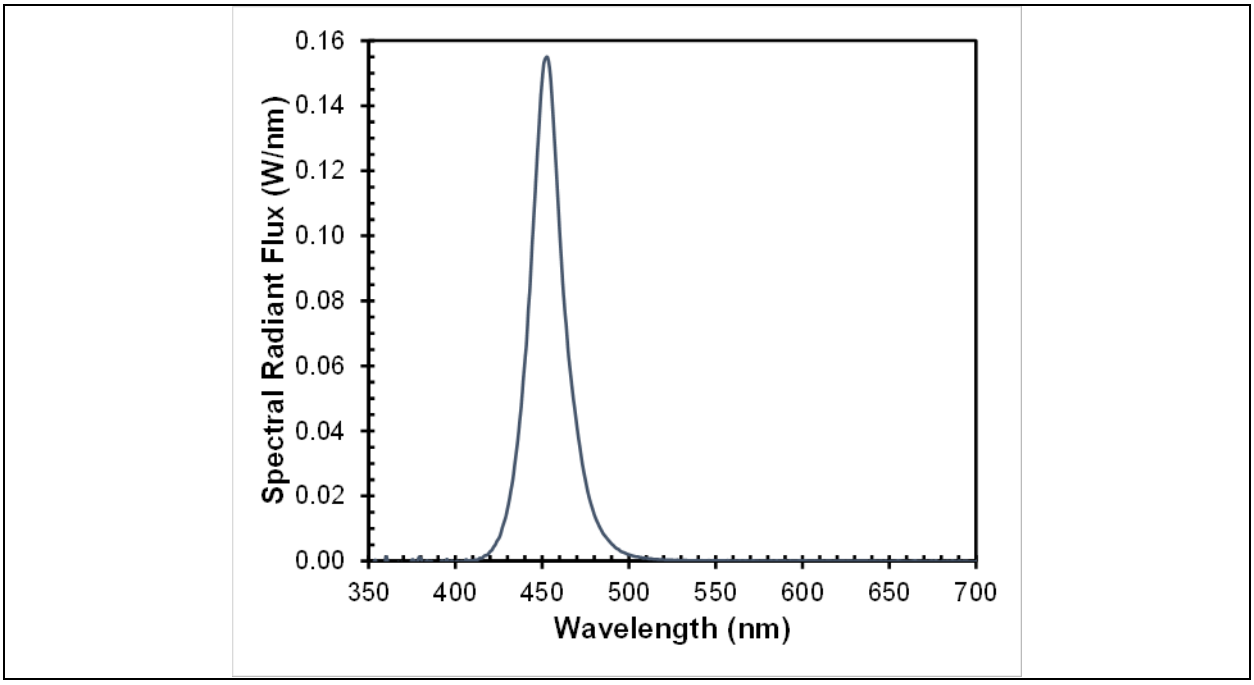

Figure D-4: SPD of Product MS-4 after phosphor removal by decapping.

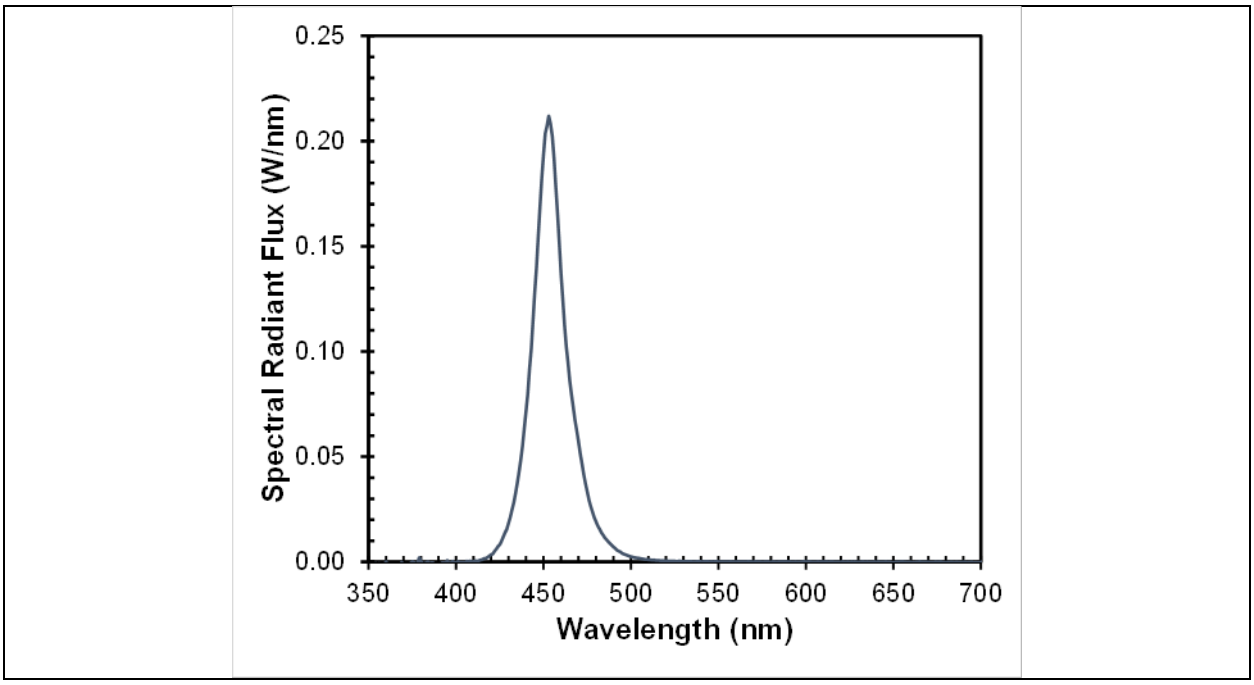

Figure D-5: SPD of Product MS-5 after phosphor removal by decapping.

(This page intentionally left blank)

U.S. DEPARTMENT OF ENERGY

Office of
ENERGY EFFICIENCY & RENEWABLE ENERGY

For more information, visit:
energy.gov/eere/ssl

DOE/EE-2357 September 2021